Novel Approaches for Translational Research in Oncology: Pharmacometric Modeling of Oncolytic Virus Dynamics and a new Tyrosine Kinase Inhibitor

Dissertation

zur Erlangung des Grades des Doktors der Naturwissenschaften
der Naturwissenschaftlich-Technischen Fakultät
der Universität des Saarlandes

von
Melanie Ines Titze
Saarbrücken
2017

Tag des Kolloquiums: 18.12.2017

Dekan: Prof. Dr. G. Kickelbick

Berichterstatter: Prof. Dr. T. Lehr

Prof. Dr. N. Graf

Vorsitzender: Prof. Dr. C. Jacob

Akad. Beisitzerin: Dr. S. Keßler

Die vorliegende Arbeit wurde von Januar 2013 bis August 2017 unter Anleitung von Herrn Professor Dr. Thorsten Lehr in der Fachrichtung Klinische Pharmazie der Naturwissenschaftlich-Technischen Fakultät der Universität des Saarlandes angefertigt.

The fear of the Lord is the beginning of knowledge

Papers included in this thesis

I **A generic viral dynamic model to systematically characterize the interaction between oncolytic virus kinetics and tumor growth**
Melanie I. Titze, Julia Frank, Michael Ehrhardt, Sigrun Smola, Norbert Graf, Thorsten Lehr
Eur. J. Pharm. Sci. 97 (2017) 38-46. doi: 10.1016/j.ejps.2016.11.003

II **A comprehensive pharmacokinetic/pharmacodynamics analysis of the novel IGF1R/INSR inhibitor BI 893923 applying in vitro, in vivo and in silico modeling techniques**
Melanie I. Titze, Otmar Schaaf, Marco H. Hofmann, Michael P. Sanderson, Stephan K. Zahn, Jens Quant, Thorsten Lehr
Cancer Chemother. Pharmacol. 77 (2016) 1303-1314. doi:10.1007/s00280-016-3049-z

III **An allometric pharmacokinetic/pharmacodynamics model for BI 893923, a novel IGF-1 receptor inhibitor**
Melanie I. Titze, Otmar Schaaf, Marco H. Hofmann, Michael P. Sanderson, Stephan K. Zahn, Jens Quant, Thorsten Lehr
Cancer Chemother. Pharmacol. 79 (2017) 545-558. doi:10.1007/s00280-017-3252-6

Contribution report

The author would like to declare her contributions to the publications I-III included in this thesis.

I The author developed the viral dynamic model and performed the simulation analysis. She conceptualized and wrote the manuscript.

II The author conducted the modeling and simulation studies, conceived and wrote the manuscript.

III The author performed the modeling and simulation analysis. She conceptualized and wrote the manuscript.

Contents

Abbreviations

Abbreviation	Definition
AIC	Akaike information criterion
CV	coefficient of variation
EGFR	Epidermal growth factor receptor
FDA	Food and Drug Administration
FO	First-order
FOCE	First-order conditional estimates
FOCE-I	First-order conditional estimates with interaction
GOF	Goodness of fit
ICA	Individual compartmental analysis
IGF	Insulin-like growth factor
IGF1R	Insulin-like growth factor 1 receptor
IIV	Interindividual variability
INSR	Insulin receptor
IOV	Interoccasional variability
NDV	Newcastle disease virus
NLME	Nonlinear mixed-effects
OF_{ELS}	Extended least square objective function
OFV	Objective function value
OV	Oncolytic virus
PD	Pharmacodynamics
pIGF1R	Phosphorylated insulin-like growth factor 1 receptor
PK	Pharmacokinetics
PV	Parvovirus
RV	Reovirus
RSE	Relative standard error
RUV	Residual variability
TK	Tyrosine kinase
TKI	Tyrosine kinase inhibitor
VPC	Visual predictive check

continued...

Abbreviation	Definition
WHO	Word Health Organization
-2LL	Minus two times the log likelihood

end

1 Graphical Abstract

$$\frac{dTumor(t)}{dt} = Gr \cdot Tumor(t) - Td \cdot Tumor(t) - \beta \cdot Tumor(t) \cdot OV(t)$$

$$\frac{dTumor(t)}{dt} = \frac{\lambda_0 \cdot Tumor(t)}{\left[1 + \left(\frac{\lambda_0}{\lambda_1} \cdot Tumor(t)\right)^{\psi}\right]^{\frac{1}{\psi}}}$$
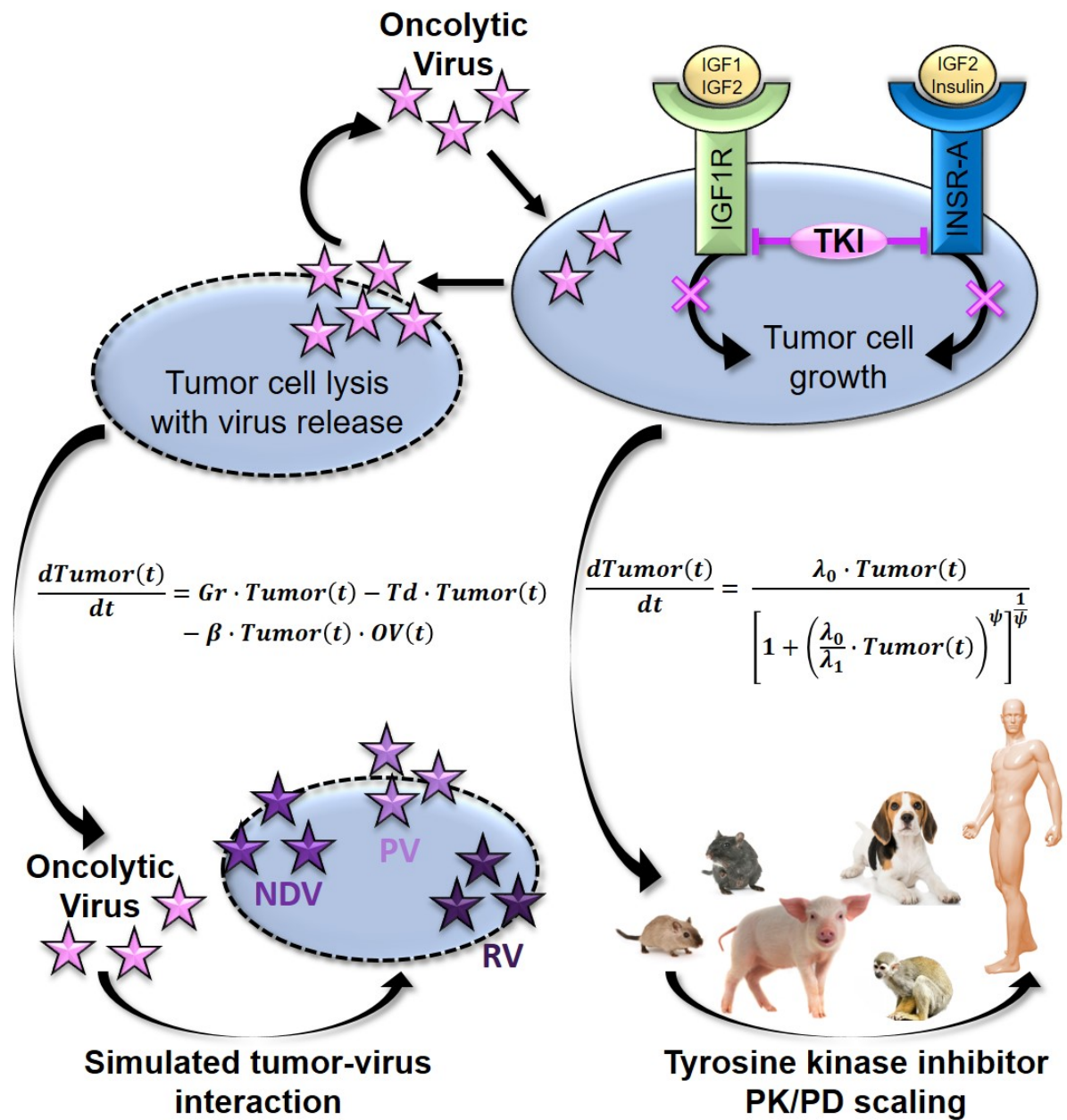
2 Introduction

2.1 Cancer

Cancer summarizes several heterogenous diseases which are characterized by a rapid and abnormal cell growth with the potential to invade neighboring tissues and to spread through the blood and lymphatic system to other organs. It comprises various molecular and cellular subtypes and can affect almost every part of the body. Although some cancer types have high cure rates by now, if they are diagnosed early and treated according to best current practice, cancer is the second leading cause of death worldwide with 8.8 million deaths in 2015[1]. Lung, liver, colorectal, stomach and breast cancer cause most cancer deaths and the American Cancer Society expects that 600,920 Americans will die of cancer in 2017, which are about 1,650 people daily[2]. The Word Health Organization (WHO) assumes an increase of 70% in the number of new cancer cases over the next 20 years[1]. Thus, there is an urgent demand for the development of new anticancer drugs and therapy strategies. Besides surgery, radiotherapy and conventional chemotherapy, the concept of immunotherapy by oncolytic viruses (OV) and the targeted therapy by receptor tyrosine kinase inhibitors (TKIs) are offering new treatment options to cure or considerably prolong life of patients.

2.2 Oncolytic viruses

Oncolytic viruses are replication-competent viruses with the ability to specifically infect and kill tumor cells whilst healthy cells are spared. Two types of OV are known: i) naturally-occurring animal-hosted viruses with innate tumor lysis capacities and no or only weak human pathogenicity and ii) genetically engineered oncolytic viruses which are virulent to tumor cells only but cannot replicate in normal human cells[3,4]. OVs exploit exactly those tumor-specific alterations which promote abnormal cell growth and thus lead to tumor cell necrosis or apoptosis. Thereby, cancer cells serve as endogenous bioreactors for virus replication and the release of new virus particles leads to an infection of surrounding tumor cells resulting in a continuous process of repeated tumor infection, cell death and virus release[3–5] (figure 2.1). Thus, an increase in virus exposure offers the potential of low initial OV doses. However, the tumor cell lysis eventuates in a self-limitation of OV production due to a decreased availability of bioreactors for further virus amplification.

2
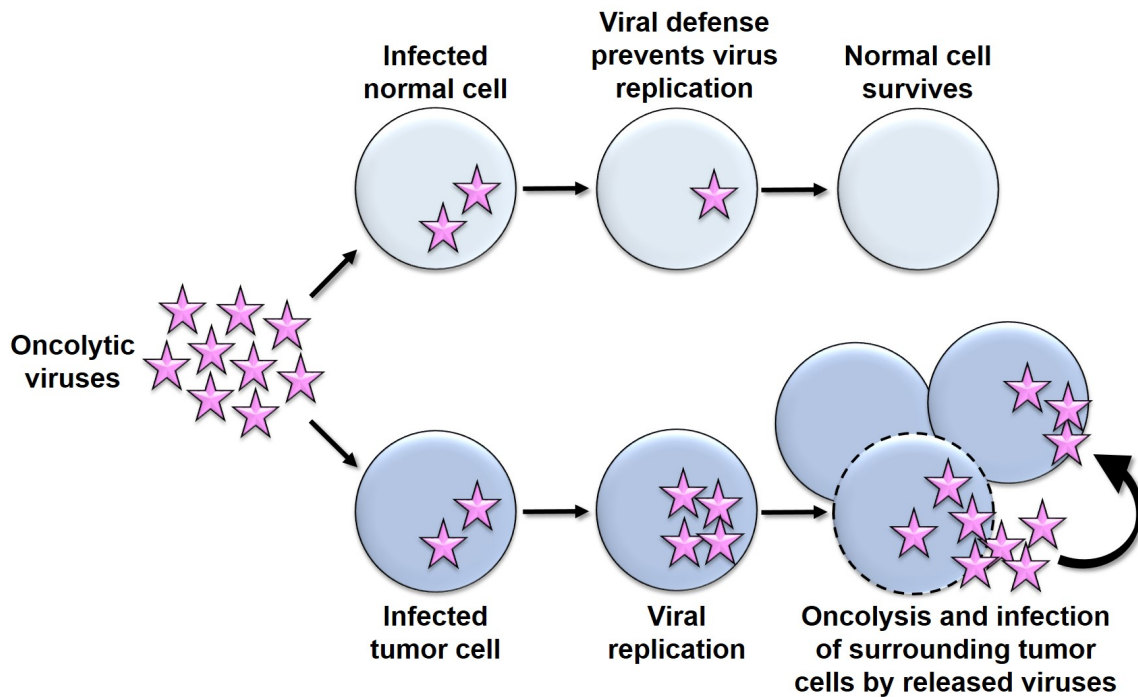
Figure 2.1 Schematic representation of oncolytic virus infection of normal and tumor cells. Whilst the antiviral defense in normal cells prevents a virus replication and cells will survive undamaged, tumor cells fail to suppress virus replication. This leads to tumor cell lysis and release of progeny virus particles which infect neighboring tumor cells and amplify the virus infection.

Several oncolytic viruses have already entered clinical trials[6] and in 2015 the genetically engineered herpes virus Imlygic® (talimogene lapharevec) was approved in the USA and Europe for the treatment of advanced melanoma[7,8]. For the naturally oncolytic viruses Newcastle disease virus (NDV), reovirus (RV) and parvovirus (PV) strong oncolytic capacities against glioma have been described *in vitro* and *in vivo*[4,9].

NDV is an enveloped single-stranded RNA virus of 150-300 nm size and the lentogenic NDV strain Hitcher B1 causes mild respiratory diseases in chicken and turkeys. Since virus replication depends on the deficient interferone signaling pathway in tumor cells, in healthy human cells interferon-induced antiviral proteins block the production of viral components at different levels of the viral replication cycle[10,11].

RV is a non-enveloped virus with double-stranded RNA genome and forms particles with a size of 60-90 nm. Its name, which is an acronym of "respiratory enteric orphan", indicates

that a RV infection is manifested by respiratory and gastrointestinal diseases but the course of the infection is in most cases asymptomatic. The type III dearing stream is under clinical development and its replication dependents on ras-mediated signaling transduction which is activated in most human cancers[6,12].

The non-enveloped PV is a single-stranded DNA virus and induces cell death mainly due to apoptosis[13], whereby its oncolytic activity seems to depend on the loss of genetic stability in cancer cells[14]. Parvoviruses are with only 20-25 nm the smallest existing viruses.

The lifecycle of OVs is influenced by their ability to self-replicate, the availability of tumor cells for virus production but also by the host immune system which on the one hand may foster the antitumoral effect but also limits the ongoing virus replication and spread[6,15]. Thus, OVs have unique pharmacokinetic properties which need to be understood and quantified for a successful translation of OVs from the culture dish to preclinical models and finally to the clinic.

2.3 Small molecule tyrosine kinase inhibitors

The era of targeted therapy started with the development of the Bcr-Abl tyrosine kinase inhibitor Imatinib for the treatment of chronic myelogenous leukemia[16,17]. By now, about 90 human tyrosin kinases (TK) are known, which are involved in the regulation of multiple processes such as cellular proliferation, differentiation and survival[18]. Abnormal TK functions are associated with the development and progression of cancer and thus a major focus in cancer research has been on the development of several TK inhibitors[18,19].

Increasingly attention has been paid to the insulin-like growth factor 1 receptor (IGF1R), a receptor tyrosine kinase which was found to play a key role in oncogenic transformation and tumorgenesis[20–22]. Binding of the natural ligands insulin-like growth factor (IGF) 1 and 2 to the extracellular domain results in receptor autophosphorylation (pIGF1R) and activation of mitogenic and anti-apoptotic downstream cascades[23]. IGF1R is structurally and functionally related to the insulin receptor (INSR) isoforms INSRA and INSRB[23]. While INSRA is mainly expressed in tumor cells and binds IGF2 and insulin to foster tumor cell proliferation and survival, INSRB is responsible for glucose uptake in metabolic tissue such as skeletal muscle, hepatocytes and adipocytes. Anticancer strategies to block the IGF signaling system comprise antibodies against the ligands IGF 1 and 2[24], IGF1R antibodies[25] and dual IGF1R/INSR tyrosine kinase inhibitors[26–28]. Since INSR can compensate for IGF1R to stimulate tumor cell growth[29,30] IGF1R antibody mediated efficacy is limited and

clinical trials with IGF1R antibodies were discouraging[31,32]. Thus a dual IGF1R/INSR inhibition by small molecule TKIs may lead to an increased anti-tumor efficacy[33] and indeed, some IGF1R/INSR TKIs have been already investigated in clinical trials[34]. However, transient hyperglycemia due to INSRB inhibition has been reported as a relevant safety issue in animals and humans[26,35,36] (figure 2.2) and needs to be addressed appropriately.
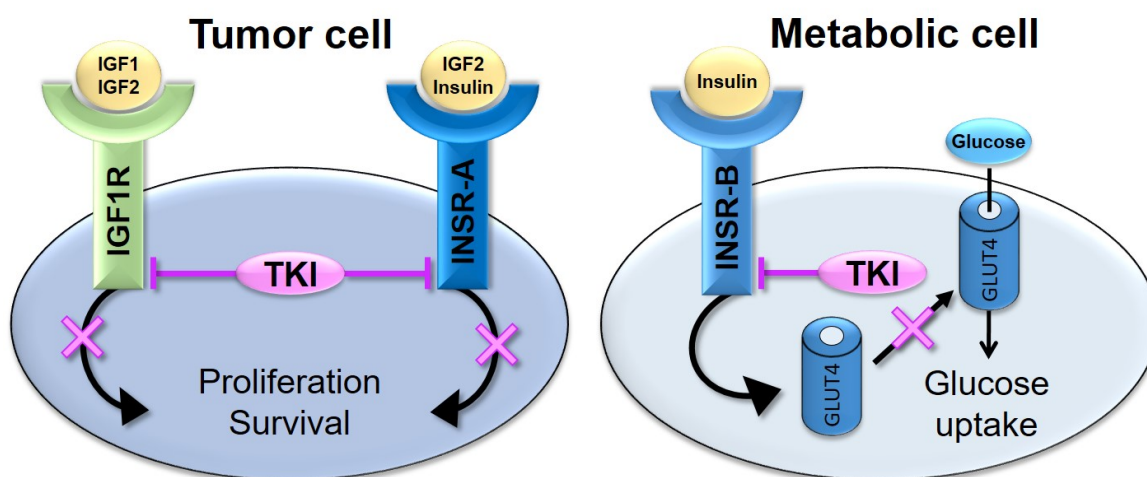
Figure 2.2 Schematic representation of the IGF1R and INSR signaling pathway in tumor and metabolic cells. In the absence of a TKI an IGF1R and INSR-A activation by IGF1, IGF2 or insulin results in cell growth and survival stimulation in tumor cells. In metabolic cells the insulin mediated activation of INSR-B induces the translocation of the GLUT4 transporter to the cell surface to enable glucose uptake into the cell. While in tumor cells the binding of the TKI at the intracellular domain of IGF1R and INSR-A results in cell cycle arrest and apoptosis, the TKI mediated inhibition of INSR-B in metabolic cells hampers the glucose uptake and evokes transient hyperglycemia.

BI 893923 is a novel potent and selective IGF1R/INSR tyrosine kinase receptor inhibitor with a molecular weight of 501 g/mol, beneficial drug-like properties and good tolerability in the mouse model. For a safe and effective use of BI 893923 as new anti-cancer therapeutic in humans, a dose selection based on a quantitative assessment of the anti-tumor efficacy against the risk of hyperglycemia will be essential.

2.4 Obstacles in cancer drug development

Despite these exciting and promising new approaches to target tumor cells by oncolytic viruses or IGF1R/INSR TKIs, the translation of preclinical findings to the clinic is still diffi-

cult with a clinical success rate in the development of new anti-cancer drugs of only 5%[37]. Major causes for the attrition are a lack of efficacy and safety accounting for about 60% of failures[37]. Already the successful translation of *in vitro* compound potency to the *in vivo* setting is hampered due to the artificial nature of cultured cell lines and because they are grown for many generations failing to reveal the natural state of the tumor[38]. Further, cultured cells fail to embrace the complete genetic tumor heterogeneity and cannot represent the complex cellular and architectural nature of tumors comprising of stroma, blood vessels and immunocompetent cells[38]. Although xenograft models consist of stroma components, this is not of human nature and furthermore, the environment and interaction between a subcutaneous tumor and the host is different compared to the tumor in its original tissue. Essential genetic, molecular, immunologic and cellular differences between mice and men may lead to translational limitations and the complex processes of human carcinogenesis, physiology and progression are inadequately reflected by animal models[39,40]. Especially pharmacokinetic differences between human and mouse are leading to a failure of safety and efficacy translation from animal studies to clinical testing[41].

2.5 Pharmacometric modeling in cancer drug development

To overcome drug development failures due to safety issues and lack of efficacy and to foster the successful translation of preclinical findings to human, the main objective is to improve the transferability of pharmacokinetics (PK) and pharmacodynamics (PD) between species. This can be realized by pharmacometric modeling[41,42], which is based upon a comprehensive understanding of the disease and therapeutic approach by considering the mechanism of drug action. It mechanistically characterizes the relationship between the administered dose, drug concentration in plasma and biophase (PK) and further the biomarker modulation as well as drug effects and side-effects (PD). Thus, pharmacometric modeling incorporates data on drug properties, the target, pathway modulation as well as pharmacology and safety[43]. Accounting for species differences, translational pharmacometric modeling allows an extrapolation of the pharmacological response to human based on the exposure-response relationship in animals[44]. The Food and Drug Administration (FDA) explicitly suggests the utilization of model-based drug development by pharmacometric analysis since translational pharmacometric modeling allows an improved clinical trial design, supports the optimization of the dosing regimen, decreases the number of animal studies and thus reduces overall costs[43,45]. From 2000 to 2008 the number of sub-

missions where pharmacometric modeling was applied increased by 6-fold, whereof 13% of submissions were in the therapeutic area of oncology[46]. In more than 60% of submissions where pharmacometric analyses were utilized, they influenced drug approval and labeling decisions and in those submissions where pharmacometric modeling contributed to drug approval decision, about 50% of reviews provided pivotal or supportive insights into effectiveness and safety[46]. Meanwhile, pharmacometric analyses play a central role in regulatory decision making by improving drug development knowledge management. Thus, pharmacometric modeling can serve as a valuable tool to foster the translation of the new anticancer concepts of oncolytic viruses and the TKI BI 893923 to the clinic.

3 Aims of this thesis

The main objective of this thesis was to foster the development of new anti-cancer drugs by supporting the translation at the preclinical-clinical interphase via pharmacometric modeling exemplarily at the concepts of oncolytic viruses and the TKI BI 893923.

Due to the exceptional pharmacokinetic features of oncolytic viruses, an encompassing understanding of the complex relation between tumor growth and virus replication is indispensable to characterize the efficacy of a certain oncolytic virus and to identify optimal dosing regimens. Hence, the aim of the first part of this theses was to develop a generic viral dynamic model to describe the bidirectional interaction between tumor growth of U87 glioblastoma cells and the viral dynamics of the three different oncolytic viruses NDV, RV and PV in an *in vitro* setting. It was further aimed to apply the established model for virus potency characterizations and for simulations of different dosing scenarios for an extended period of time to identify the optimal dosing scheme for follow up studies.

As the dual inhibition of IGF1R/INSR by the selective TKI BI 893923 is another encouraging new treatment approach, the potential dose-limiting metabolic intolerabilities due to transient hyperglycemia needs to be addressed appropriately. Thus, for a successful transition to clinic a comprehensive understanding of the relationship between BI 893923 plasma concentration and the desired effect of IGF1R blockade with resulting tumor growth inhibition as well as the undesired effect of hyperglycemia will be crucial to maximize the therapeutic window of this agent. Hence, in the second part of the thesis it was aimed to develop a population PK/PD model for the novel TKI BI 893923 to describe its plasma concentration, pIGF1R biomarker modulation and resulting tumor growth inhibition as well as blood glucose levels in mice. The established model should be used for dose adjustment simulations in mice to counterbalance tumor growth inhibition versus the risk of hyperglycemia.

In the third part of this thesis it was aimed to translate the developed mouse PK/PD for BI 893923 to human by allometric scaling of PK and blood glucose, as surrogate PD endpoint, using data from mouse, rat, dog, minipig and monkey. In addition, it was intended to conduct a comprehensive risk-benefit analysis for humans to balance anti-tumor efficacy and metabolic toxicity in order to support the human therapeutic dose estimation by a rational recommendation of an optimal efficacious dosing scheme.

4 Methods

4.1 Pharmacometric drug-disease modeling

4.1.1 Background

Pharmacometics describes the development and application of mathematical and statistical models to characterize, understand and predict a drugs PK and PD. Thus, it supports rational, data-driven decisions in drug development, regulatory approval and pharmacotherapy. Pharmacokinetics describes the fate of a drug in the body and characterizes the relationship between the administered drug and drug concentration by absorption, distribution, metabolism and elimination processes. The plasma concentration-time profile can be depicted by compartmental PK modeling where the body is divided in several pharmacokinetically distinct compartments which correspond to the number of distribution phases[47]. The pharmacological effect of a drug on the body can be described by pharmacodynamics[48]. It characterizes the relationship between the drug concentration and the pharmacological effects and the relationship of those responses to clinical outcomes. PD markers can be biomarker measurements (*e.g.* level of receptor activation) or efficacy and toxicity outcomes such as tumor growth inhibition or level of hyperglycemia, respectively. The drug effect in dependency of the drug concentration can be described by various well-established PD models such as simple linear models or the often applied Emax-Model[49].

PK/PD modeling describes the drug exposure and drug effect over time and enables the assessment of desired and undesired drug effects in dependency of drug exposure. It helps to understand the dose-exposure-effect relationship to support preclinical and clinical drug development as well as dose finding for a safe and efficacious use.

4.1.2 The population approach

To describe the PK and PD of a drug, every individual can be analyzed separately using the individual compartmental analysis (ICA). However, more complex processes might not be identified in single individuals and generalized statements about a population of individuals can be more reliably derived using the population approach. This method describes the typical PK and PD profile of a population and quantifies the variability within this population[50]. Large datasets from different experiments and studies can be combined and

analyzed together whereby the experiment design can vary with respect to sampling time and number of observations. Three different population approaches can be distinguished:

- The naïve pooled analysis combines data from all individuals and estimates the typical model parameters, whilst variability between individuals is not considered[51].

- The standard two-stage approach estimates in the first step model parameters for each individual separately using the ICA and calculates in the second step the mean and percentiles to quantify the variability between individuals[52]. With this approach the source of variability cannot be identified, leading to a systematic overestimation of variability within the population since the calculated variability represents both interindividual and residual variability[53]. Further, a complete plasma concentration-time profile for each individual is needed (data-rich situation) and a balanced study design is necessary.

- In nonlinear mixed-effects (NLME) modeling all individual measurements are analyzed simultaneously and the typical PK and PD profiles as well as the variability within a population are described. PK and PD variability within a population can be adequately quantified and distinguished in interindividual, interoccasional and residual variability[51,52]. Further, individual specific characteristics (covariates) such as body weight can be considered and quantitatively related to certain model parameters to explain and reduce variability. This method can be used for unbalanced study designs due to pooled experiments and in data-sparse situations when few or only one measurement per individual is available, for instance when animals had to be scarified for determination of biomarker levels. Due to the superiority of NLME modeling, this approach was applied in this thesis and will be described in detail in the following section.

4.1.3 Nonlinear mixed-effects modeling

The NLME modeling approach denotes a particular kind of nonlinear regression analysis in which the observed data (plasma drug concentrations or PD readouts) are described by a mathematical function (model) which is a nonlinear combination of the model parameters[54]. The term "mixed-effects" results from the simultaneous estimation of "fixed effects", representing population parameters and covariate effects and "random effects", accounting for unexplainable intra- and interindividual variability as well as residual variability[55].

A NLME-model consists of three hierarchical components: i) the structural model describing the typical PK or PD profile for the population, ii) the statistical model, which quantifies the unexplained variability within this population and iii) an optional covariate model, which explains part of the variability by individual-specific characteristics (covariates). A general expression of a NLME model is shown in equation 4.1:

$$Y = f(\theta, x, z, \Omega, K, \Sigma) \tag{4.1}$$

The observations Y are described by the function $f()$, which determines the mathematical structure of the model and contains θ, which is the vector of the typical population parameters. x denotes the vector of the independent design parameters (*e.g.* dose, time) and z the optional vector of individual-specific covariates. The random variability parameters are defined by the matrices Ω, K and Σ which represent the interindividual, interoccasional and residual variability, respectively.

4.1.3.1 Structural model

The structural model describes the typical PK or PD profile at a given time as function of model parameters and should reflect the general tendency of the observations. It is developed in a sequential manner, starting with the simplest model and proceeding to more complex ones by including additional parameters to capture all essential system features. PK/PD models are developed in a step-wise process by first defining a final PK model and then generating the PD model.

4.1.3.2 Pharmacostatistical model

The statistical model describes the variability of a structural parameter θ_k within a population due to random effects and allows the estimation of individual parameters *e.g.* individual clearance CL for an individual i. The variability quantified in the statistical model may result from differences between various individuals (interindividual variability, IIV) or from variations within one individual at different occasions (interoccasional variability, IOV), which will not be further explained as it was not analyzed within this work. The remaining discrepancy between the observations and model predictions is defined as unexplainable residual variability (RUV), which may result from analytical errors, model misspecifications or other factors.

Interindividual variability To account for the fact that parameters in a population are often log-normal (right-skewed) distributed and to prevent the occurrence of negative and

thus non-physiological parameter estimates the IIV is often modeled as an exponential relationship:

$$P_{ki} = \theta_k \cdot e^{\eta_{ki}} \tag{4.2}$$

where P_{ki} is the individual structural parameter and η_{ki} the difference between the natural logarithm of P_{ki} and the typical population value θ_k. It is assumed that η_{ki} is independently, symmetrically distributed with zero mean and a variance ω_k^2. The variance represents the diagonal element of the variance-covariance-matrix Ω and can be reported as coefficient of variation (CV) which is calculated as:

$$CV[\%] = \sqrt{e^{\omega_k^2} - 1} \cdot 100\% \tag{4.3}$$

Although, in theory variability is plausible for every parameter, a dataset does not always contain sufficient information for a reliable quantification of the variability. Thus, the decision to include the IIV was based on the objective function value (OFV, section 4.1.5.1), the precision and the relevance of the estimated value itself.

Residual variability   The remaining deviation between individual model predictions and observations is considered as random and was investigated by the following three implementations to describe the RUV.

- Additive error model:

$$y_{ij} = f(\phi_i, X_{ij}) + \varepsilon_{add,ij} \tag{4.4}$$

- Proportional error model:

$$y_{ij} = f(\phi_i, X_{ij}) \cdot (1 + \varepsilon_{prop,ij}) \tag{4.5}$$

- Combined error model:

$$y_{ij} = f(\phi_i, X_{ij}) \cdot (1 + \varepsilon_{prop,ij}) + \varepsilon_{add,ij} \tag{4.6}$$

y_{ij} is the measured observation of the i-th individual at time j, $f(\phi_i, X_{ij})$ represents the individual model prediction and $\varepsilon_{add,ij}$ and $\varepsilon_{prop,ij}$ quantify the random difference between y_{ij} and $f(\phi_i, X_{ij})$. It is assumed that ε_{ij} is distributed symmetrically with mean zero and a variance σ^2, which represents the diagonal element of the Σ matrix. The additive error model assumes that the variance is constant over the whole range of observations, which

is often the case for measurements with narrow range such as PD readouts. The standard deviation of the additive residual variability is given by $\sqrt{\sigma^2_{add}}$ and has the same unit as the observation. The proportional error model is applied if the variance is dependent on the magnitude of the observations and proportionally increases with higher values, as this is typically the case for drug concentration. $\sqrt{\sigma^2_{prop} \cdot 100}$ represents the coefficient of variation of the proportional residual error in %. The combined error model merges the additive and proportional error model. Thus, for small observations the additive residual variability component dominates and for higher values this error model will behave like a proportional error model. The final RUV model was selected based on plausibility and criteria for model selection (section 4.1.5).

4.1.3.3 Covariate model

The covariate model describes the impact of certain individual-specific characteristics on PK and PD parameters with the aim to explain and reduce the IIV. These variables can be continuous such as body weight or creatinine clearance and integrated in the model as a linear, exponential or power function[47]. Covariates can further be categorical (dichotomous or classified) such as sex or age range and enter the model in an additive, fractional or exponential way. Covariate integration was investigated based on plausibility and graphical screening and decided by the OFV (section 4.1.5.1) and precision.

4.1.4 Estimation methods

In population modeling it is aimed to identify the set of model parameters, which best describes the observed data. There are several software packages available to estimate NLME models, one of them is NONMEM®[56], which was used within this thesis. The algorithm implemented in NOMNEM® iteratively searches for the set of parameters that maximize the probability that the observations were adequately reproduced. Instead of maximizing the likelihood-function, NONMEM® iteratively seeks for the global minimum of minus two times the logarithm of the likelihood $-2LL$, which is called the objective function value (OFV). To approximate the function $-2LL$, the method of extended least square objective function OF_{ELS}[57] is used (equation 4.7).

$$OF_{ELS} = \sum_{i=1}^{n} \left[\frac{(y_i - E(y_i))^2}{var(y_i)} + \ln |var(y_i)| \right] \tag{4.7}$$

Assuming an additive residual error model, y_i represents the vector of observations and $E(y_i)$ the vector of model prediction for y_i. $var(y_i)$ is the variance-covariance matrix for y_i, which includes all variability parameter and weights the squared residual error $(y_i - E(y_i))^2$. For an infinite number of variance parameters the OF_{ELS} could become infinitely small, which is prevented by a penalty term for every additional variance $\ln|var(y_i)|$[51]. Due to the nonlinear relation between observations and parameter estimates there is no closed-form solution for the OF_{ELS} and the minimum cannot be calculated analytically. To overcome this issue, a Taylor series approximation can be applied to determine the minimal OFV. Within this work two general methods implemented in NONMEM® were used: the first order approximation (FO) and first-order conditional estimation (FOCE) method[57]. To approximate the solution of the function in both methods the model function is linearized into a first-order polynomial of the first partial derivative of the function and the function itself with respect to the random variables η and ε. For the FO method the Taylor series approximation is solved by several iterative steps under the assumption of $\eta = 0$, considering only the population parameters. The individual parameter estimates (conditional estimates) are then assessed *a posteriori* using the Bayesian estimation method[58]. In contrast, for the FOCE method the iterative solutions for θ and η are estimated at every iteration step simultaneously and thus the population estimates and the respective individual parameters (conditional estimates) are obtained in parallel to every iteration step and are not estimated *a posteriori*. The FOCE method can be refined by the INTERACTION option (FOCE+I), which considers a correlation between the residual and interindividual variability. Since the interaction option can be neglected only for additive residual error models, this option was applied for all modeling analysis within this work. In general, for model development within this thesis the FO method was used since it converges considerably faster and final models were estimated with FOCE+I, as this method provides more precise parameter estimates[59]. Besides the deterministic FO and FOCE method other estimation algorithms are available in NONMEM, which are the Laplacian Approximation (LAPLACE) or stochastic Monte Carlo expectation-maximization (EM) methods such as Monte-Carlo importance sampling (IMP), IMP assisted by mode a posteriori estimation (IMPMAP) or the stochastic approximation expectation maximization (SAEM) method, which are more valuable for more complex PK/PD models.

4.1.5 Model selection and evaluation

To assess a models descriptive and predictive performance and to compare different kinds of models several numerical and graphical tools can be applied.

4.1.5.1 Objective function value and Akaike information criterion

To test for a statistical significant model improvement during model building, the likelihood ratio test can be applied, if models are nested. Models are denoted as nested when the complex model can be reduced to a simpler model by omitting one or more parameters[47]. The OFVs for both models are compared whereby the difference in the OFV is approximately χ^2-distributed[47]. Thus, for one additional parameter (degree of freedom (df)=1) the difference in the OFV has to be at least 3.84 points to be statistical significant at a given level of significance of 0.05. To numerically compare non-nested models the Akaike Information Criterion (AIC)[47] can be applied, which uses a penalty term for every additional parameter P. The AIC can be calculated as

$$AIC = -2 \cdot LL + 2 \cdot P \tag{4.8}$$

4.1.5.2 Relative standard error

The relative standard error (RSE) can be used to assess the precision of parameter estimates, where a smaller RSE is associated with a higher precision. During the covariance step NONMEM® estimates the absolute standard error of parameters from the square route of the diagonal elements of the variance-covariance matrix. The RSE is then calculated from the absolute standard error as follows

$$RSE = \frac{absolute\ standard\ error}{parameter\ estimate} \cdot 100\% \tag{4.9}$$

Another method to determine the RSE is the bootstrap method[60]. For this method a sufficient high number of new datasets with the same sample size as the original dataset is generated by randomly sampling and replacing individuals from the original dataset. For every new dataset model parameters are determined and the variance of all parameter estimates can be calculated, assuming normally distributed parameters. The square route of the variance is equal to the absolute standard error and thus, the RSE can be calculated according to equation 4.9.

4.1.5.3 Graphical methods

Graphical analysis can be used to visually assess the goodness of fit (GOF) and to detect model misspecifications. During model development the following GOF plots have been routinely generated using the SAS® software version 9.4[61]:

- Measured observations versus population or individual predictions

- Weighted residuals versus population or individual predictions

- Weighted residuals versus time or time after dose

Weighted residuals are the weighted differences between measured observations and population or individual predictions, respectively. Using the FOCE+I method, the estimation of conditional weighted residuals is possible, which results in more meaningful statements about error model[62]. Ideally all points should be scattered closely, randomly and uniformly around the line of identity for observations versus population or individual predictions plots and around the zero line for residual plots.

4.1.5.4 Visual predictive check

The visual predictive check (VPC) is a simulation based tool to graphically evaluate the predictive power of a model by assessing the accordance of model predictions with observations[63,64]. Based on the final model and under original study design sufficiently high numbers of simulations (≥ 500) were performed. The subsequently calculated 90% prediction interval of the simulated values is then compared to observed data, where the simulated median should reflect the median of the observations. The variability is accurately reflected by the model when 5% of observations are below and above the 5th and 95th percentile, respectively.

4.1.6 Simulations

4.1.6.1 Deterministic simulations

Deterministic simulations consider only the structural parameters of a model whereby the variability is neglected. Investigating the typical PK and PD profiles can be helpful to explore the influence of covariates on the PK and PD and to gain insights into the structural model[47].

4.1.6.2 Stochastic simulations

For stochastic simulations all sources of variability are considered and thus the predicted model responses (*e.g.* plasma concentration or tumor growth) represent the reality more accurately and reveal the range of the expected outcome. By randomly sampling sets of model parameters from the multivariate distribution and subsequent computation of corresponding PK and PD profiles the variability within a population is included. Since stochastic simulations are the method of choice when several dose regimens are investigated for their safety and efficacy outcome and suggestions for dose-optimization need to be derived, they were applied for simulation analysis within this thesis. Stochastic simulations can be further used for internal model validation (VPC, section 4.1.5.4).

5 Results

5.1 Publication I: A generic viral dynamic model to systematically characterize the interaction between oncolytic virus kinetics and tumor growth (doi: 10.1016/j.ejps.2016.11.003)

5.2 Publication II: A comprehensive pharmacokinetic/pharmacodynamics analysis of the novel IGF1R/INSR inhibitor BI 893923 applying in vitro, in vivo and in silico modeling techniques (doi:10.1007/s00280-016-3049-z)

5.3 Publication III: An allometric pharmacokinetic/pharmacodynamics model for BI 893923, a novel IGF-1 receptor inhibitor (doi:10.1007/s00280-017-3252-6)

6 Conclusions

Currently, many new innovative cancer therapeutics are under investigation, such as self-replicating oncolytic viruses and small molecule TKIs, which rise hope for an improved tumor therapy and eventually a cure. However, translation of efficacy and safety from *in vitro* to *in vivo* and then to clinical trials remains difficult with a low rate of success, partly due to bad preclinical experiment design but also due to differences in interspecies pharmacology and pharmacokinetics[40,41]. Thus, there is an urgent need to foster early drug development and to evolve new strategies for an improved translational research. Since many studies fail to adequately relate anti-tumor response to required human drug exposure[41], it is believed that the application of pharmacometric modeling in preclinical drug development could considerably improve efficiency and success of drug research by enabling a sophisticated extrapolation of animal PK and PD to human under consideration of interspecies differences[42]. Therefore, translational pharmacometric modeling provides a solid support to cancer drug development when it is applied in early stage development[65,66], which was demonstrated by the examples of oncolytic viruses and the TKI BI 893923 within this thesis.

For the three OVs NDV, RV and PV a generic OV model with a joint structure was developed which describes at the same time tumor growth and virus replication considering the complex bi-directional tumor-virus interaction. The developed virus dynamics model can be expanded to other OVs and tumor cell lines beyond the ones tested here and could be further universally employed to cross-characterize various virus-tumor relations. The virus dynamics model was successfully used to simulate the long-term tumor-virus interrelation and to predict tumor reoccurrence for different dosing scenarios. A treatment rating score was developed, which enabled a preselection of the most promising oncolytic virus within the optimal dosing regimen for the design of *in vivo* experiments. In the future the model can be further utilized to characterize *in vitro* tumor growth kinetics for tumor cells obtained from patient biopsies to predict the most promising virus strain and dosing regimen for the individual patient.

For the novel IGF1R/INSR TKI BI 893923 a PK/PD model was developed, which successfully described the relationship between BI 893923 plasma concentration, pIGF1R biomarker modulation as well as resulting tumor growth inhibition and blood glucose levels in mice. The model was used to simulate different dosing regimens with the result of an improved safety window with respect to hyperglycemia and increased anti-tumor efficacy for dosing

every 8 hours compared to once-daily dosing. The PK/PD model successfully supported the preclinical process and dose optimization in mice and could prospectively be employed for comparison and evaluation of different IGF1R/INSR TKIs.

For accurate predictions of the human therapeutic dose the BI 893923 PK/PD model was successfully scaled across mouse, rat, dog, minipig and monkey by allometric principles and extrapolated to human. External predictions of monkey PK and blood glucose, as surrogate PD endpoint, confirmed the transferability of the model across various species and supported the reliability of the human predictions. To broaden the therapeutic window in human with increased anti-tumor efficacy and reduced duration of hyperglycemia, various dosing schedules were simulated and a comprehensive risk-benefit analysis was conducted. Based on the net clinical benefit for each schedule an optimal human dose of 2750 mg BI 893923 every 8 hours was predicted. The here presented allometric PK/PD model successfully supported the transferability of safety and efficacy at the preclinical-clinical interface and thus substantially impacted the successful development of a new innovate anti-cancer drug. In the future, the model could be used to evaluate other IGF1R/INSR TKI and to test combination therapies of BI 893923 with other anticancer drugs such as inhibitors of the epidermal growth factor receptor (EGFR) or MEK as well as conventional cytotoxic agents[67–69]. To further optimize the metabolic tolerability, combinations with anti-diabetic drugs such as metformin could be performed[70,71] and the model could be applied to other anti-cancer drugs associated with hyperglycemia such as PI3K-AktmTOR pathway inhibitors[72].

In summary, the projects within this thesis demonstrated the successful application of pharmacometric modeling in preclinical oncolytic drug development. Utilizing information and data at different stages of the drug discovery process enabled the development and application of predictive models to direct future experiment design and decision making. As basis for translational research, pharmacometric modeling supported the transferability of drug safety and efficacy based on rational, data driven suggestions and provided the foundation for dose-optimization.

7 Summary

Despite many innovative anti-cancer drugs in the pipeline, the attrition rate for anti-tumor drugs is high due to a lack of predictability of efficacy and safety from *in vitro* settings to animal models and at the preclinical-clinical interphase. In this thesis pharmacometric modeling was applied to support early cancer drug development exemplary for the concepts of oncolytic viruses (OV) and the tyrosine kinase inhibitor (TKI) BI 893923. For OV therapy a understanding of the bi-directional tumor-virus interaction is essential. Thus, a generic viral dynamic model was developed based on *in vitro* data from Newcastle disease virus, reovirus and parvovirus for the treatment of U87 glioblastoma cells, which simultaneously describes tumor growth and virus kinetics. The model was used for a depiction of virus efficacy and selection of optimal dose regimens. BI 893923 is a novel TKI of the insulin-like growth factor 1 receptor (IGF1R) and insulin receptor (INSR) with promising anti-tumor efficacy. Since for other IGF1R/INSR inhibitors dose-limiting hyperglycemia was reported, a mouse PK/PD model was developed, relating BI 893923 plasma concentration to biomarker modification and tumor growth as well as blood glucose to balance anti-tumor efficacy with the risk of hyperglycemia. The model was scaled to human by allometric principles using data from mouse, rat, dog, minipig and monkey and a risk-benefit analysis was conducted to determine the optimal safe and efficient human dose.

8 Zusammenfassung

Trotz intensiver Forschung in der Onkologie ist die Zahl neuer Zulassungen gering, da die Übertragbarkeit von Wirksamkeit und Sicherheit von *in vitro* Tests auf Tiermodelle und an der präklinisch-klinischen Schnittstelle nur ungenügend ist. Um die Entwicklung zu unterstützen, wurden in dieser Arbeit am Beispiel von onkolytischen Viren (OV) und des Tyrosinkinaseinhibitors (TKI) BI 893923 pharmakometrische Modelle entwickelt. Für die Therapie mit OV ist ein Verständnis der wechselseitigen Tumor-Virus-Beziehung essentiell. Daher wurde basierend auf *in vitro* Newcastle disease-, Reo-und Parvovirusdaten zur Behandlung von U87 Glioblastomzellen ein generisches Virus-Dynamik-Modell entwickelt, welches simultan Tumorwachstum und Viruskinetik beschreibt. Das Modell wurde zur Bestimmung von Viruseffizienz und optimaler Dosierungsregime genutzt. BI 893923 ist ein neuer TKI des Insulin-like Growth Faktor 1 Rezeptors (IGF1R) und Insulin Rezeptors (INSR). Da für andere IGF1R/INSR TKIs dosislimitierende Hyperglykämien berichtet wurden, wurde ein Maus PK/PD Model entwickelt, welches die BI 893923 Plasmakonzentration, Biomarkermodifikation, das Tumorwachstum und die Blutglukose beschreibt, um die antitumorale Wirksamkeit gegen das Hyperglykämierisiko abzuwägen. Es wurden Daten von Maus, Ratte, Hund, Minischwein und Affe genutzt um das Modell allometrisch auf den Menschen zu skalieren und es wurde eine Risiko-Nutzen-Analyse durchgeführt, um eine sichere und wirksame humane Dosis zu bestimmen.

9 Bibliography

[1] URL `http://www.who.int/mediacentre/factsheets/fs297/en/` (accessed May 20, 2017).

[2] URL `https://www.cancer.org/cancer/cancer-basics/economic-impact-of-cancer.html` accessed June 01, 2017).

[3] M. Roberts, R. Lorence, W. Groene and M. Bamat. Naturally oncolytic viruses. *Curr Opin Mol Ther*, 8: 314–21 (2006).

[4] A. Haseley, C. Alvarez-Breckenridge, A.R. Chaudhury and B. Kaur. Advances in oncolytic virus therapy for glioma. *Recent Pat CNS Drug Discov*, 4: 1–13 (2009).

[5] K.A. Parato, D. Senger, P.A.J. Forsyth and J.C. Bell. Recent procress in the battle between oncolytic viruses and tumours. *Nat Rev Cancer*, 5: 965–976 (2005).

[6] D. Kirn, R.L. Martuza and J. Zwiebel. Replication-selective virotherapy for cancer: Biological principles, risk management and future directions. *Nat Med*, 7: 781–787 (2001).

[7] R.H.I. Andtbacka, H.L. Kaufman, F. Collichio, T. Amatruda, N. Senzer, Chesney J., et al. Talimogene laherparepvec improves durable response rate in patients with advanced melanoma. *J Clin Oncol*, 33: 2780–2788 (2015).

[8] H. Ledford. Cancer-fighting viruses win approval. *Nature*, 526: 622–623 (2005).

[9] M. Alkassar, B. Gärtner, K. Roemer, F. Graesser, J. Rommelaere, L. Kaestner, et al. The combined effects of oncolytic reovirus plus Newcastle disease virus and reovirus plus parvovirus on U87 and U373 cells in vitro and in vivo. *J Neurooncol*, 104: 715–727 (2011).

[10] V. Schirrmacher, K. Jurianz, C. Roth, A. Griesbach, R. Bonifer, R. Zawatzky. Tumor stimulator cell modification by infection with Newcastle Disease Virus: analysis of effects and mechanism in MLTC-CML cultures. *Int J Oncol*, 14: 205–215 (1999).

[11] C. Fiola, B. Peeters, P. Fournier, A. Arnold, M. Bucur, V. Schirrmacher. Tumor selective replication of Newcastle disease virus: association with defects of tumor cells in antiviral defence. *Int J Cancer*, 119: 328–338 (2006).

[12] J.E. Strong, M.C. Coffey, D. Tang, P. Sabinin and Patrick W.K. Lee. The molecular basis of viral oncolysis: Usurpation of the Ras signaling pathway by reovirus. *EMBO J*, 17: 3351–3362 (1998).

[13] B. Bauder, A. Suchy, C. Gabler and H. Weissenböck. Apoptosis in Feline Panleukopenia and Canine Parvovirus Enteritis. *J Vet Med*, 47: 775–784 (2000).

[14] P.K. Singh, J. Doley, G.R. Kumar, A.P. Sahoo and A.K. Tiwari. Oncolytic viruses their specific targeting to tumour cells. *Indian J Med Res*, 136: 571–584 (2012).

[15] T. Todo, S.D. Rabkin, P. Sundaresan, A. Wu, K.R. Meehan H.B. Herscowitz, et al. Systemic Antitumor Immunity in Experimental Brain Tumor Therapy Using a Multimutated, Replication-Competent Herpes Simplex Virus. *Hun Gene Ther*, 10: 2741–2755 (1999).

[16] B.J. Druker, C.L. Sawyer, H. Kantarjian, D.J. Resta, S.F. Reese, J.M. Ford, et al. Activity of a specific inhibitor of the Bcr-Abl Tyrosine kinase in the blast crisis of chronic myeloid leukemia and acute lymphoblastic leukemia with the Philadeslphia chromosome. *N Engl J Med*, 344: 1038–1042 (2001).

[17] B.J. Druker, S. Tamur, E. Buchdunger, S. Ohno, G.M. Segal, S. Fanning, et al. Effects of a selective inhibitor of the Abl tyrosine kinase on the growth of Bcr-Abl positve cells. *Nat Med*, 2: 561–566 (1996).

[18] D.S. Krause and R.A. Van Etten. Tyrosine Kinases as Targets for Cancer Therapy. *N Engl J Med*, 353: 172–187 (2005).

[19] K. Takeuchi and F. Ito. Receptor Tyrosine Kinases and Targeted Cancer Therapeutics. textitBiol Pharm Bull, 34: 1774–1780 (2011).

[20] C. Sell, M. Rubini, R. Rubin, J. Liut, A. Efstratiadist and R. Baserga. Simian virus 40 large tumor antigen is unable to transform mouse embryonic fibroblasts lacking type 1 insulin-like growth factor receptor. *Proc Natl Acad Sci USA*, 90: 11217–11221 (1993).

[21] M. Pollak. The insulin and insulin-like growth factor receptor family in neoplasia: an update. *Nat Rev Cancer*, 12: 159–169 (2012).

[22] F. Peruzzi, M. Prisco, M. Dews, P. Salomoni, E. Grassilli, G. Romano, et al. Multiple Signaling Pathways of the Insulin-Like Growth Factor 1 Receptor in Protection from Apoptosis. *Mol Cell Biol*, 19: 7203–7215 (1999).

[23] P. De Meyts, J. Palsgaard, W. Sajid, A.-M. Theede and H. Aladdin. Structural biology of insulin and IGF-1 receptors. *Nat Rev Drug Discov*, 1: 769–783 (2002).

[24] K. Friedbichler, M.H. Hofmann, M. Kroez, E. Ostermann, H.R. Lamche, C. Koessl, et al. Pharmacodynamic and Antineoplastic Activity of BI 836845, a Fully Human IGF Ligand-Neutralizing Antibody, and Mechanistic Rationale for Combination with Rapamycin. *Mol Cancer Ther*, 13: 399–409 (2014).

[25] P.J. Beltran, P. Mitchell, Y.-A Chung, E. Cajulis, J. Lu, B. Belmontes, et al. AMG 479, a fully human anti-insulin-like growth factor receptor type I monoclonal antibody, inhibits the growth and survival of pancreatic carcinoma cells. *Mol Cancer Ther*, 8: 1095–1105 (2009).

[26] J.M. Carboni, M. Wittman, Z. Yang, F. Lee, A. Greer, W. Hurlburt, et al. BMS-754807, a small molecule inhibitor of insulin-like growth factor-1R/IR. *Mol Cancer Ther*, 8: 3341–3349 (2009).

[27] M. Jin, J. Wang, E. Buck and M.J. Mulvihill. Small-molecule ATP-competitive dual IGF-1R and insulin receptor inhibitors: structural insights, chemical diversity and molecular evolution. *Future Med Chem*, 4: 315–328 (2012).

[28] A. Negi, P. Ramarao, R. Kumar. Recent Advancements in Small Molecule Inhibitors of Insulin-like Growth Factor-1 Receptor (IGF-1R) Tyrosine Kinase as Anticancer agents. *Mini-Rev Med Chem*, 13: 653–681 (2013).

[29] E. Buck and M. Mulvihill. Small molecule inhibitors of the IGF-1R/IR axis for the treatment of cancer. *Expert Opin Investig Drugs*, 20: 605–621 (2011).

[30] A. Louvi, D. Accili and A. Efstratiadis. Growth-promoting interaction of IGF-II with the insulin receptor during mouse embryonic development. *Dev Biol*, 189: 33–48 (1997).

[31] R. Osborne. Commercial interest waxes for IGF-1 blockers. *Nat Biotechnol*, 26: 719–720 (2008).

[32] D. Yee. Insulin-like Growth Factor Receptor Inhibitors: Baby or the Bathwater? *J Natl Cancer Inst*, 104: 975–981 (2012).

[33] E. Buck, P.C. Gokhale, S. Koujak, E. Brown, A. Eyzaguirre, N. Tao, et al. Compensatory Insulin Receptor (IR) Activation on Inhibition of Insulin-Like Growth Factor-1

Receptor (IGF-1R): Rationale for Cotargeting IGF-1R and IR in Cancer. *Mol Cancer Ther*, 9: 2652–2664 (2010).

[34] H. King, T. Aleksic, P. Haluska and V.M. Macaulay. Can we unlock the potential of IGF-1R inhibition in cancer therapy? *Cancer Treat Rev*, 40: 1096–105 (2014).

[35] C.R. Becerra, R. Salazar, R. Garcia-Carbonero, A.L. Thomas, F.J. Vázquez-Mazón, J. Cassidy, et al. Figitumumab in patients with refractory metastatic colorectal cancer previously treated with standard therapies: a nonrandomized, open-label, phase II trial. *Cancer Chemother Pharmacol*, 73: 695–702 (2014).

[36] I. Puzanov, C.R. Lindsay, L. Goff, J. Sosman, J. Gilbert and J. Berlin. A phase I study of continuous oral dosing of OSI-906, a dual inhibitor of insulin-like growth factor-1 and insulin receptors, in patients with advanced solid tumors. *Clin Cancer Res*, 21: 701–711 (2015).

[37] I. Kola and J. Landis. Can the pharmaceutical industry reduce attrition rates? *Nat Rev Drug Discov*, 3: 717–716 (2004).

[38] A. Kamb. What's wrong with our cancer models? *Nat Rev Drug Discov*, 4: 161–165 (2005).

[39] J.C.L. Schuh. Trials, Tribulations, and Trends in Tumor Modeling in Mice. *Toxicol Pathol*, 32: 53–66 (2004).

[40] I.W. Mak, N. Evaniew and M. Ghert. Lost in translation: animal models and clinical trials in cancer treatment. *Am J Transl Res*, 6: 114–8 (2014).

[41] J.K. Peterson and P.J. Houghton. Integrating pharmacology and in vivo cancer models in preclinical and clinical drug development. *Eur J Cancer*, 40: 837–844 (2004).

[42] B.M. Agoram, S.W. Martin and P.H. Van Der Graaf. The role of mechanism-based pharmacokinetic-pharmacodynamic (PK – PD) modelling in translational research of biologics. *Drug Discov Today*, 12: 1018–1024 (2007).

[43] T. Lavé, A. Caruso, N. Parrott and A. Walz. Translational PK/PD modeling to increase probability of success in drug discovery and early development *Drug Discovery Today Technol*, 21-22: 27-34 (2016).

[44] D.E. Mager and W.J. Jusko. Development of translational pharmacokinetic-pharmacodynamic models. *Clin Pharmacol Ther*, 83: 909–12 (2008).

[45] T. Tuntland, B. Ethell, T. Kosaka, F. Blasco, R.X. Zang, M. Jain, et al. Implementation of pharmacokinetic and pharmacodynamic strategies in early research phases of drug discovery and development at Novartis Institute of Biomedical Research. *Front Pharmacol*, 5: 174 (2014).

[46] J.Y. Lee, C.E. Garnett, J.V. Gobburu, V.A. Bhattaram, S. Brar, J.C. Earp, et al. Impact of pharmacometric analyses on new drug approval and labelling decisions: a review of 198 submissions between 2000 and 2008. *Clin Pharmacokinet*, 50: 627–635 (2011).

[47] P.L. Bonate (Hrsg.). *Pharmacokinetic-pharmacodynamic modelling and simulation*. Springer, New York, second edition (2011).

[48] P. Lees, F.M. Cunningham and J. Elliott. Principles of pharmacodynamics and their applications in veterinary pharmacology. *J Vet Pharmacol Ther*, 27: 397–414 (2004).

[49] N.H.G. Holford and L.B. Sheiner. Kinetics of pharmacologic response. *Pharmac Ther*, 16: 143–166 (1982).

[50] S.B. Duffull, D.F.B. Wright and H.R. Winter. Interpreting population pharmacokinetic-pharmacodynamic analyses – a clinical viewpoint. *Br J Clin Pharmacol*, 71: 807–814 (2011).

[51] L.B. Sheiner and S.L. Beal. Evaluation of Methods for Estimating Population Pharmacokinetic Parameters. I. Michaelis-Menten Model: Routine Clinical Pharmacokinetic Data. *J Pharmacokinet Biopharm*, 8: 553–571 (1980).

[52] L.B. Sheiner and S.L. Beal. Evaluation of Methods for Estimating Population Pharmacokinetic Parameters II. Biexponential Model and Experimental Pharmacokinetic Data. *J Pharmacokinet Biopharm*, 9: 635–651 (1981).

[53] J. Steimer, A. Mallet, J. Golmard and J.-F. Boisvieux. Alternative Approaches to Estimation of Population Pharmacokinetic Parameters: Comparison with the Nonlinear Mixed-Effect Model. *Drug Metab Rev*, 15: 265–292 (2008).

[54] L.B. Sheiner. Analysis of Pharmacokinetic Data Using Parametric Models–l: Regression Models. *J Pharmacokinet Biopharm*, 12: 93–117 (1984).

[55] C.W. Tornøe, H. Agersø, E.N. Jonsson, H. Madsen and H.A. Nielsen. Non-linear mixed-effects pharmacokinetic/pharmacodynamic modelling in NLME using differential equations. *Comput Methods Programs Biomed*, 76: 31–40 (2004).

[56] S.L. Beal and L.B. Sheiner. *NONMEM Users Guide*. University of California (1989).

[57] S.L. Beal. Population Pharmacokinetic Data and Parameter Estimation Based on Their First Two Statistical Moments. *Drug Metab Rev*, 15: 173–193 (1984).

[58] S.L. Beal and L.B. Sheiner. *NONMEM Users Guide. Conditional Estimation Methods*. University of California (1998).

[59] Y. Wang. Derivation of various NONMEM estimation methods. *J Pharmacokinet Pharmacodyn*, 34: 575–593 (2007).

[60] B Efron. Bootstrap Methods: Another Look at the Jackknife. *Ann Stat*, 7: 1–26 (1979).

[61] SAS Institue Inc. *SAS software* (2002–2012)

[62] A.C. Hooker, C.E. Staatz and M.O. Karlsson. Conditional Weighted Residuals (CWRES): A Model Diagnostic for the FOCE Method. *Pharm Res*, 24: 2187–2197 (2007).

[63] N.H. Holford and M.O. Karlsson. A Tutorial on Visual Predictive Checks. URL `http://page-meeting.org/?abstract=1434` (accessed May 7, 2016).

[64] M.O. Karlsson and R.M. Savic. Diagnosing model diagnostics. *Clin Pharmacol Ther*, 82: 17–20 (2007).

[65] S. Suryawanshi, L. Zhang, M. Pfister and B. Meibohm. The current role of model-based drug development. *Expert Opin Drug Discov*, 5: 311–21 (2010).

[66] D.R. Mould, A-C. Walz, T. Lave, J.P. Gibbs and B. Frame. Developing Exposure/Response Models for Anticancer Drug Treatment: Special Considerations. *CPT Pharmacometrics Syst Pharmacol*, 4: e00016 (2015).

[67] S.V. Sharma, D.Y. Lee, B. Li, M.P. Quinlan, F. Takahashi, S. Maheswaran, et al. A chromatin-mediated reversible drug tolerant state in cancer cell subpopulations. *Cell*, 141: 69–80 (2010).

[68] S.A. Flanigan, T.M. Pitts, S.G. Eckhardt, J.J. Tentler, A.C. Tan, A. Thorburn, et al. The insulin-like growth factor I receptor/insulin receptor tyrosine kinase inhibitor PQIP exhibits enhanced antitumor effects in combination with chemotherapy against colorectal cancer models. *Clin Cancer Res*, 16: 5436–46 (2010).

[69] S.A. Flanigan, T.M. Pitts, T.P. Newton, G.N. Kulikowski, A. Choon, M.C. McManus, et al. Overcoming IGF1R/IR Resistance Through Inhibition of MEK Signaling in Colorectal Cancer Models. *Clin Cancer Res*, 19: 6219–6229(2013).

[70] D. Stepensky, M. Friedman, I. Raz and A. Hoffman. Pharmacokinetic-pharmacodynamic analysis of the glucose-lowering effect of metformin in diabetic rats reveals first-pass pharmacodynamic effect. *Drug Metab Dispos*, 30: 861–868 (2002).

[71] M.G. Zager, K. Kozminski, B. Pascual, K.M. Ogilvie and S. Sun. Preclinical PK/PD modeling and human efficacious dose projection for a glucokinase activator in the treatment of diabetes. *J Pharmacokinet Pharmacodyn*, 41: 127–39 (2014).

[72] N.L. Busaidy, A. Farooki, A. Dowlati, J.P. Perentesis, J.E. Dancey, L.A. Doyle, et al. Management of metabolic effects associated with anticancer agents targeting the PI3K-Akt-mTOR pathway. *J Clin Oncol*, 30: 2919–2928 (2012).

Picture credits for graphical abstract

Mouse, Rat and monkey from `www.pixabay.com/de`
Dog, minipig and human purchased from `www.fotolia.com`

10 Supporting Information

10.1 Supporting Information I: A generic viral dynamic model to systematically characterize the interaction between oncolytic virus kinetics and tumor growth

Supplemental Material to:

A generic viral dynamic model to systematically characterize the interaction between oncolytic virus kinetics and tumor growth

Model Equations:

$$\frac{dT_U(t)}{dt} = Gr \cdot T_U(t) \cdot start - Td \cdot T_U(t) - \beta \cdot T_U(t) \cdot OV(t) \qquad \text{Eq.(A.1)}$$

$$\frac{dT_I(t)}{dt} = \beta \cdot T_U(t) \cdot OV(t) - \delta \cdot T_I(t) \qquad \text{Eq.(A.2)}$$

$$\frac{dOV(t)}{dt} = \rho \cdot T_I(t) - CL \cdot OV(t) \qquad \text{Eq.(A.3)}$$

With *start* = 0 if Time <= *LAG* and *start*=1 if Time > *LAG*

and $\delta = \frac{D_{max} \cdot OV^N}{DC_{50}{}^N + OV^N}$ $\qquad \text{Eq.(A.4)}$

The initial condition at time zero for each population is defined as follows:

$$T_U(0) = 10000$$

$$T_I(0) = 0$$

$$OV(0) = 0$$

In the above equations, T_U are the uninfected tumor cells, T_I infected tumor cells and *OV* the oncolytic virus. *Gr* is the growth rate and *Td* the death rate of uninfected cells, *β* denotes the infection rate and *δ* the infected cell death rate. *δ* is calculated by a sigmoidal Emax-model, where D_{max} denotes the maximum death rate, DC_{50} the virus titer for a half-maximum death rate and *N* the hill factor. *ρ* represent the release rate for new virions and CL the rate for virus clearance. *LAG* denotes the lag-time after which uninfected cells start to grow. Tumor cells were infected with OVs 24 h after seeding.

Reproductive ratio R_0:

$$R_0 = \frac{\beta \cdot Gr \cdot \rho}{\delta \cdot Td \cdot Cl}$$

Since $\frac{Gr}{Td}$ is the same for all the viruses the constant can be canceled out, leading to

$$R_0 = \frac{\beta \cdot \rho}{\delta \cdot Cl}$$

with $\delta = \frac{D_{max} \cdot OV^N}{DC_{50}^N + OV^N}$

As δ is changing over time because it depends on the virus titer at a given time, the reproductive ratio

R_0 for a virus is also changing over time and needs to be calculated for every time point of interest.
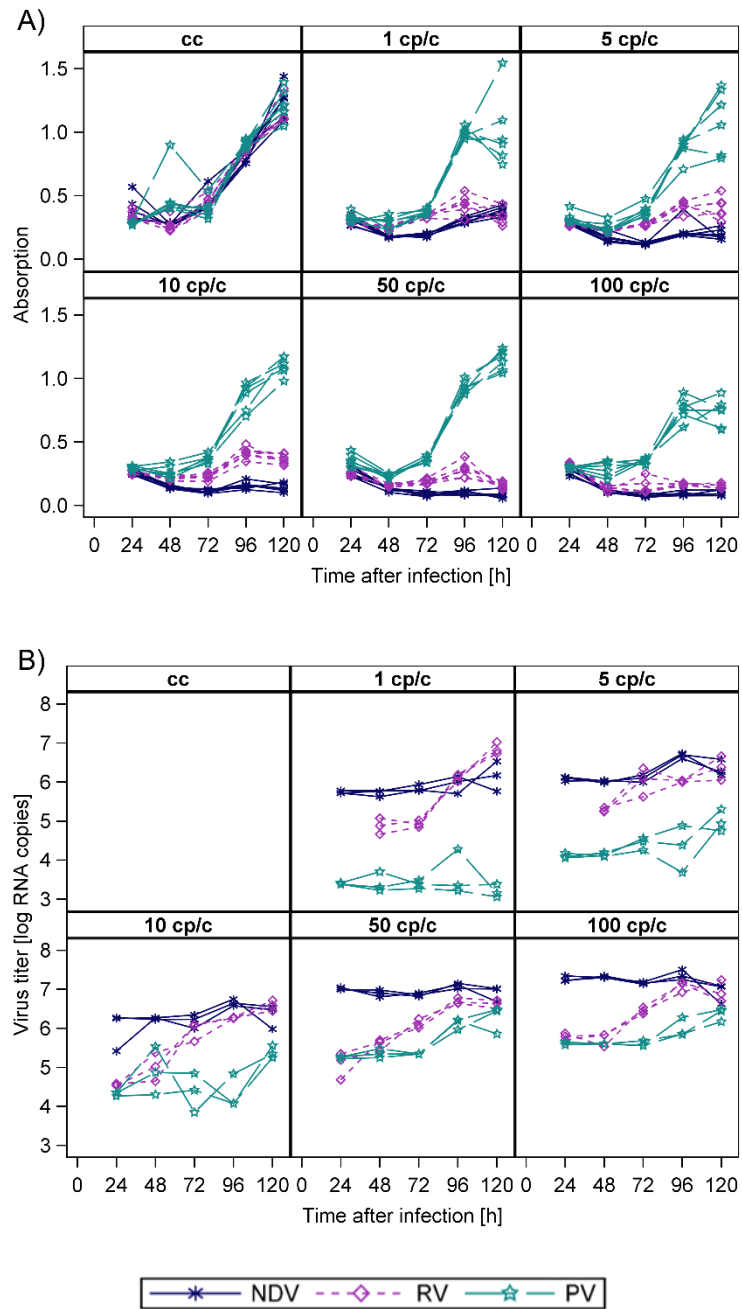
Supplementary Figure A.1: A) Measured U87 glioblastoma cell growth up to 120 h after infection.

B) Measured virus titer up to 120h after infection. cc, control group with 0 cp/c virus.
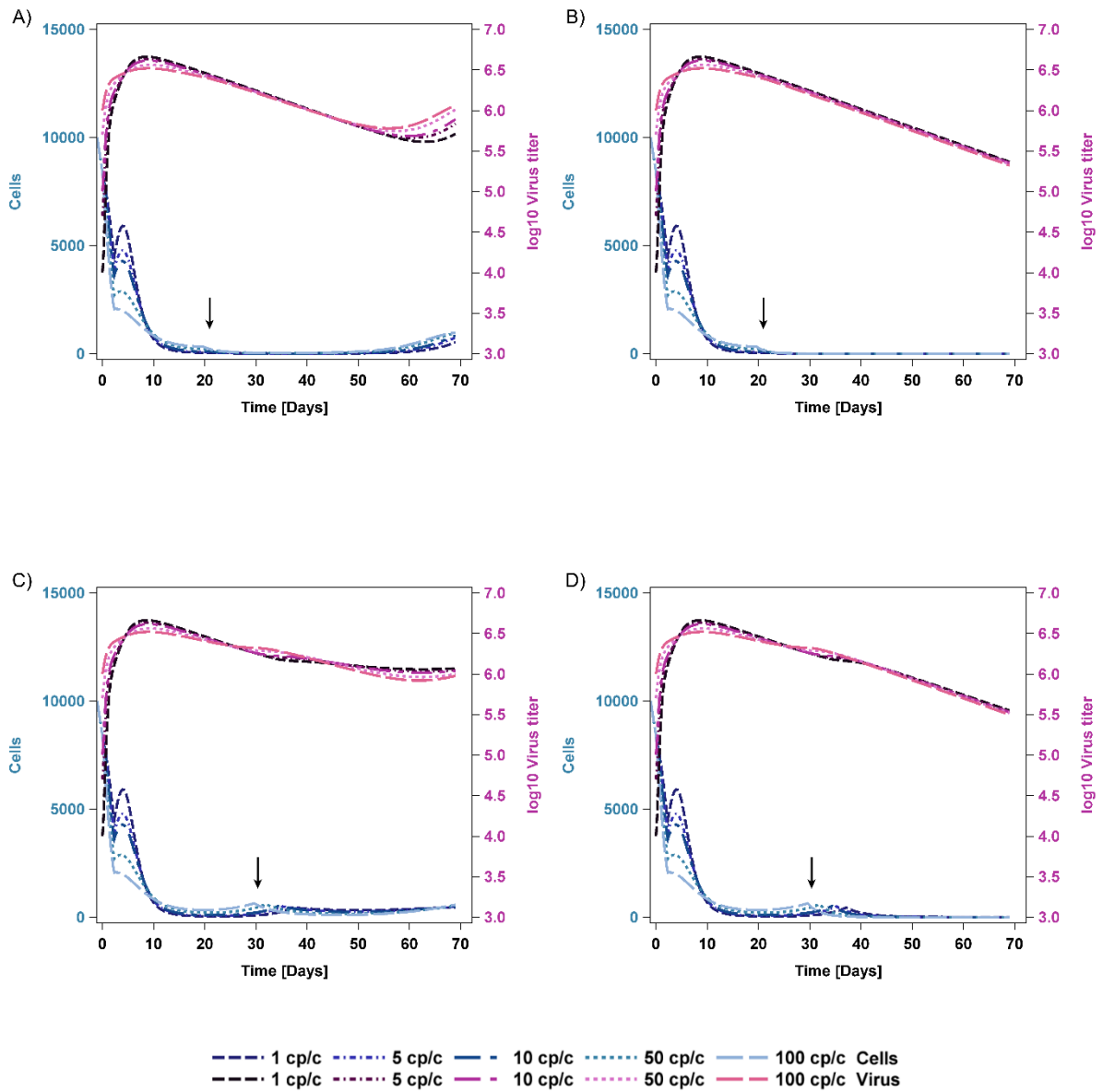
Supplementary Figure A.2: Combination of NDV treatment with a cytotoxic compound that induces

(A) 30% or (B) 60% tumor cell growth inhibition with start of treatment at tumor nadir. Additional

cytotoxic therapy starting at virus nadir with C) 30% and D) 60% growth inhibition. Arrows indicate

start of chemotherapy.

Supplementary Table A.1: Treatment rating *Score* and *EraScore* for combination of NDV with a hypothetical cytotoxic compound of 30 or 60% growth inhibition, starting chemotherapy at tumor nadir or virus nadir.

Growth inhibition started at	% Inhibition	Dose [cp/c]	*Score*	*EraScore*	Tumor Eradication
Tumor nadir	30	1	0.26	-	no
Tumor nadir	30	5	0.63	-	no
Tumor nadir	30	10	0.89	-	no
Tumor nadir	30	50	1.89	-	no
Tumor nadir	30	100	2.65	-	no
Tumor nadir	60	1	0	0.075	yes
Tumor nadir	60	5	0	0.077	yes
Tumor nadir	60	10	0	0.079	yes
Tumor nadir	60	50	0	0.083	yes
Tumor nadir	60	100	0	0.085	yes
Virus nadir	30	1	1.66	-	no
Virus nadir	30	5	3.17	-	no
Virus nadir	30	10	4.29	-	no
Virus nadir	30	50	10.32	-	no
Virus nadir	30	100	17.40	-	no
Virus nadir	60	1	1.61	-	no
Virus nadir	60	5	3.17	-	no
Virus nadir	60	10	4.29	-	no
Virus nadir	60	50	10.32	-	no
Virus nadir	60	100	0	0.139	yes
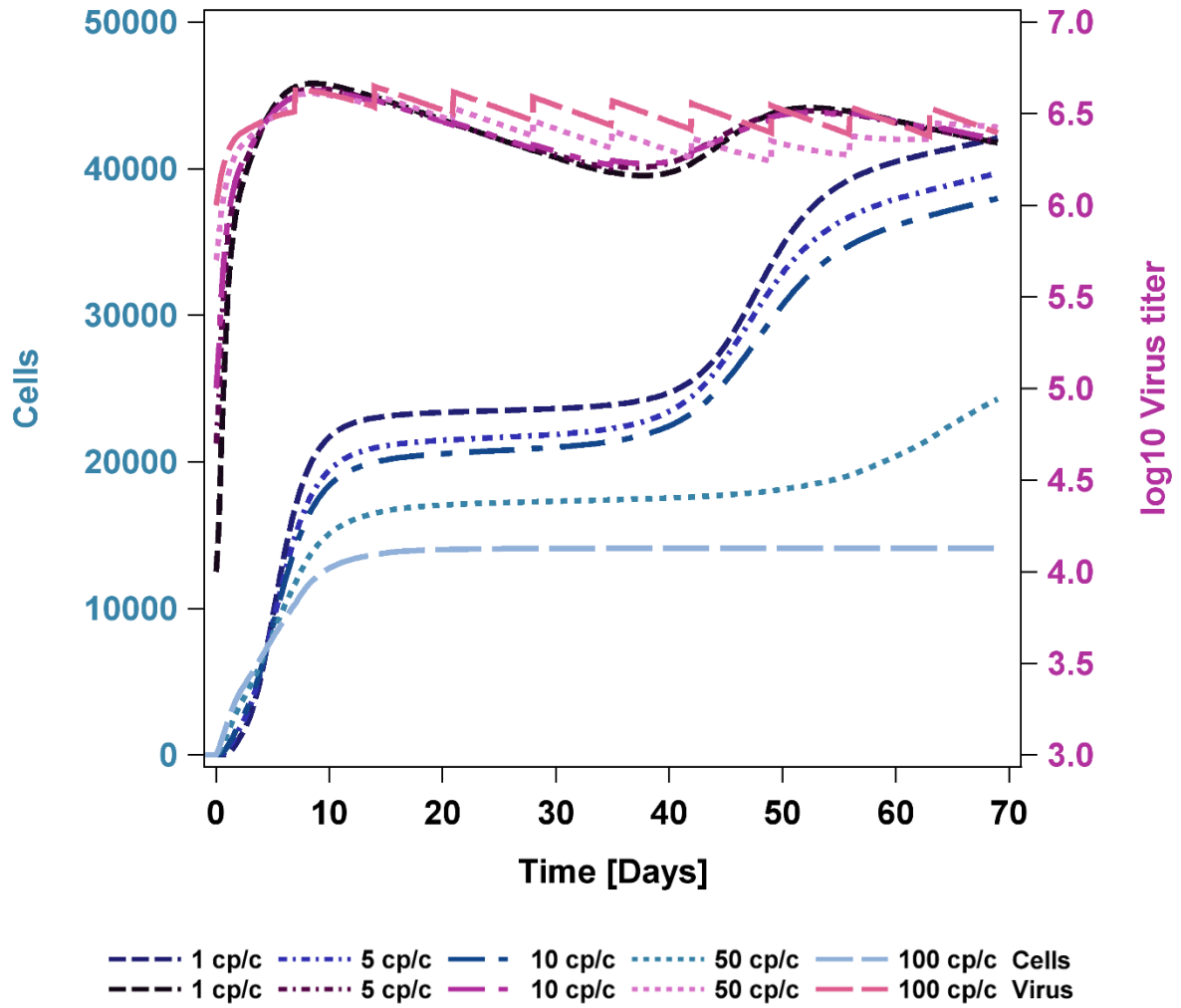
Supplementary Figure A.3: Simulation of tumor cell number (blue lines) and virus titer (violet lines)

over 10 weeks for continuous weekly dosing with NDV.

Supplementary Figure A.4: Simulation of tumor cell number (blue lines) and NDV virus titer (violet lines) over 10 weeks for various levels of tumor load A) 5000 seeded cells, B) 15000 seeded cells, C) 20000 seeded cells.
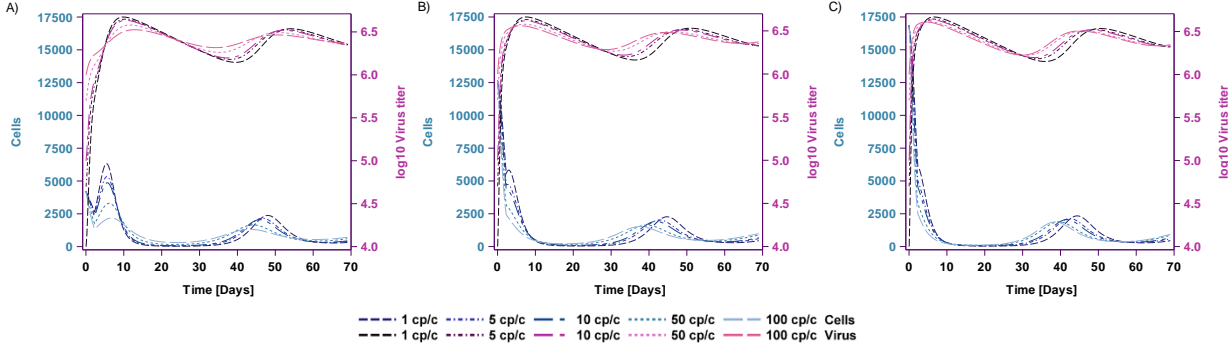
Supplementary Figure A.5: Simulation of tumor cell number (blue lines) and RV virus titer (violet lines) over 10 weeks for various levels of tumor load A) 5000 seeded cells, B) 15000 seeded cells, C) 20000 seeded cells.
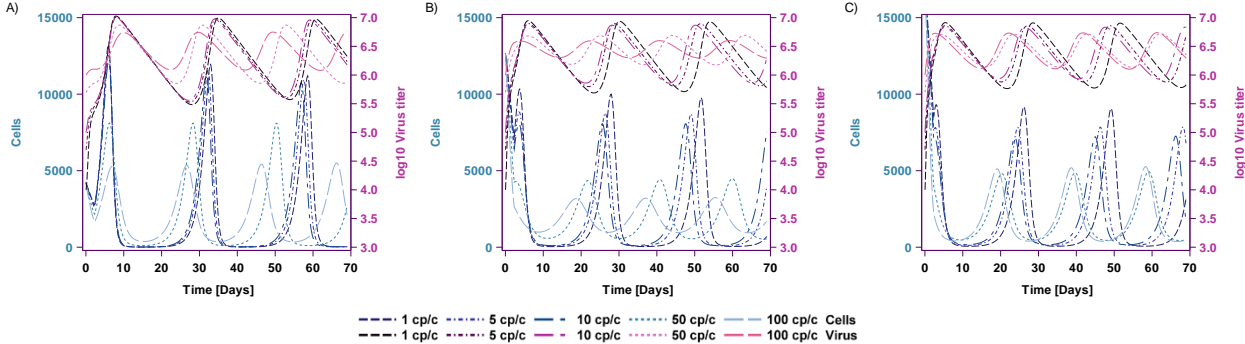
Supplementary Figure A.6: Simulation of tumor cell number (blue lines) and PV virus titer (violet lines) over 10 weeks for various levels of tumor load A) 5000 seeded cells, B) 15000 seeded cells, C) 20000 seeded cells.
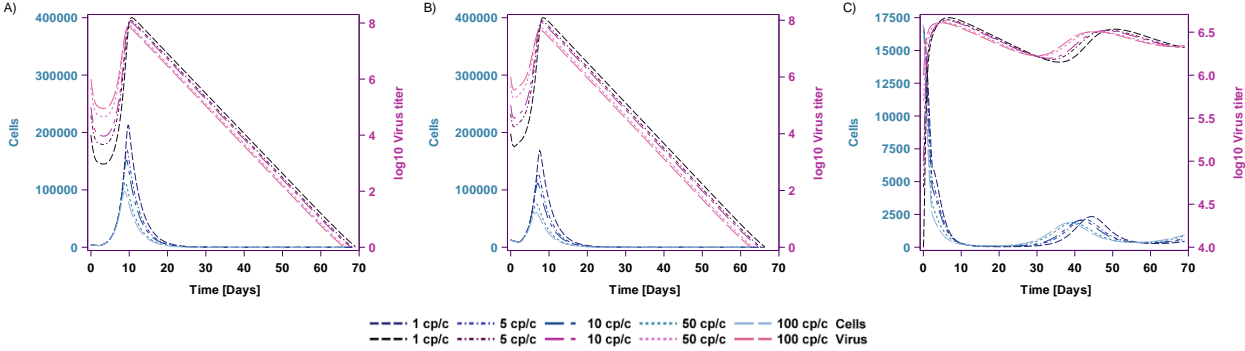
10.2 Supporting Information II: A comprehensive pharmacokinetic/pharmacodynamics analysis of the novel IGF1R/INSR inhibitor BI 893923 applying in vitro, in vivo and in silico modeling techniques

Supplemental Materials to:

A comprehensive pharmacokinetic/pharmacodynamics analysis of the novel IGF1R/INSR inhibitor BI 893923 applying *in vitro*, *in vivo* and *in silico* techniques

Melanie I. Titze[1], Otmar Schaaf[2], Marco H. Hofmann[2], Michael P. Sanderson[2], Stephan K. Zahn[2], Jens Quant[2], Thorsten Lehr[1]

[1]Clinical Pharmacy, Saarland University, Saarbrücken, Germany

[2]Boehringer Ingelheim RCV GmbH & Co KG, Vienna, Austria

Online Resource Material 1: Data characterization for PK/PD modelling

Table 1

Compressive data characterization for modelling analysis.

Model	Animals		Observations		Number of values below LLOQ*	Dose groups
	treated	control	treated	control		
PK	112	0	344	0	25	7
Biomarker	60	12	60	12	0	4
Tumor	102	26	452	138	0	5
Glucose	117	19	312	35	28	7

* LLOQ: Lower limit of quantification

Online Resource Material 2: Model equations

PK Model:

$$\frac{dA1(t)}{dt} = -KA_1 \cdot A1(t)$$

$$\frac{dA2(t)}{dt} = -KA_2 \cdot A2(t) \cdot start$$

$$\frac{dA3(t)}{dt} = KA_1 \cdot A1(t) + KA_2 \cdot A2(t) - \left(\frac{CL}{V1}\right) \cdot A3(t) - \left(\frac{Q}{V1}\right) \cdot A3(t) + \left(\frac{Q}{V2}\right) \cdot A4(t) - \left(\frac{Q2}{V1}\right)$$
$$\cdot A3(t) + \left(\frac{Q2}{V3}\right) \cdot A5(t)$$

$$\frac{dA4(t)}{dt} = \left(\frac{Q}{V1}\right) \cdot A3(t) - \left(\frac{Q}{V2}\right) \cdot A4(t)$$

$$\frac{dA5(t)}{dt} = \left(\frac{Q2}{V1}\right) \cdot A3(t) - \left(\frac{Q2}{V3}\right) \cdot A5(t)$$

With *start* = 0 if Time <= T_{lag} and *start*=1 if Time > T_{lag}

Biomarker/TGI Model:

$$\frac{dA6(t)}{dt} = K_1 \cdot \left(\frac{A3(t)}{V1}\right) - K_1 \cdot A6(t)$$

$$\frac{dA7(t)}{dt} = K_{PHOS} \cdot \left(1 - \left(\frac{A7(t)}{IC_{50} + A7(t)}\right)\right) - K_{DE-PHOS} \cdot A7(t)$$

$$\frac{dA8(t)}{dt} = K_2 \cdot \left(\frac{A7(t)}{Base}\right) - K_2 \cdot A8(t)$$

$$\frac{dA9(t)}{dt} = K_2 \cdot A8(t) - K_2 \cdot A9(t)$$

$$\frac{dA10(t)}{dt} = \frac{\lambda_{0T} \cdot A10(t)}{\left[1 + \left(\frac{\lambda_{0T}}{\lambda_{1T}} \cdot A10(t)\right)^{\psi}\right]^{\frac{1}{\psi}}}$$

With:

$$\lambda_{0T} = \lambda_0 \cdot \frac{A7(t)}{Base} \cdot A8(t) \cdot A9(t)$$

$$\lambda_{1T} = \lambda_1 \cdot \frac{A7(t)}{Base} \cdot A8(t) \cdot A9(t)$$

$\psi=20$

$$K_{PHOS} = K_{DE-PHOS} \cdot Base$$

44

Glucose Model:

$$\frac{dA11(t)}{dt} = K_{SYN} \cdot (1 + A12(t)) - K_{DISP} \cdot A11(t) \cdot \left(1 - \left(\frac{I_{maxGluc} \cdot \frac{A3(t)}{V1}}{IC_{50Gluc} + \frac{A3(t)}{V1}} \right) \right)$$

$$\frac{dA12(t)}{dt} = -\left(\frac{Q3}{V12}\right) \cdot A12(t) - \left(\frac{Q4}{V12}\right) \cdot A12(t) + \left(\frac{Q4}{V13}\right) \cdot A13(t)$$

$$\frac{dA13(t)}{dt} = \left(\frac{Q4}{V12}\right) \cdot A12(t) - \left(\frac{Q4}{V13}\right) \cdot A13(t)$$

With $K_{SYN} = K_{DISP} \cdot BL_{Gluc}$

The initial conditions at time zero for each compartment are defined as follows:

$A1(0) = Dose \cdot F1$

$A2(0) = Dose \cdot F2$

$A3(0) = A4(0) = A5(0) = 0$

$A6(0) = 0$

$A7(0) = Base$

$A8(0) = A9(0) = 1$

$A10(0) = BL$

$A11(0) = BL_{Gluc}$

$A12(0) = Placebo$

$A13(0) = 0$

With $F1 = (1 - FF2) \cdot BV_{tot}$ and $F2 = FF2 \cdot BV_{tot}$

In the above equations, A1 and A2 represent the fast and slow absorption compartments, respectively and A3 the central PK compartment. A4 and A5 reflect the peripheral compartments. A6 denotes the effect compartment and A7 the pIGF1R biomarker compartment. The biomarker transit compartments are reflected by A8 and A9 and the tumor compartment is represented by A10. A11 reflects the glucose compartment and A12 the

central placebo and A13 peripheral placebo compartment. The Placebo PK parameters were
scaled to mouse based on published human parameters [25].

Online Resource Material 3: Goodness-of-fit plots
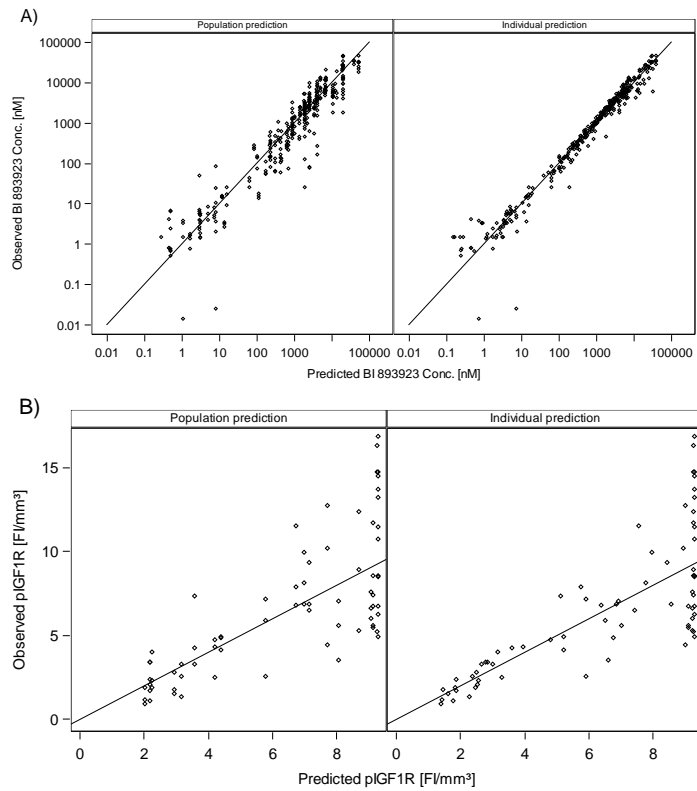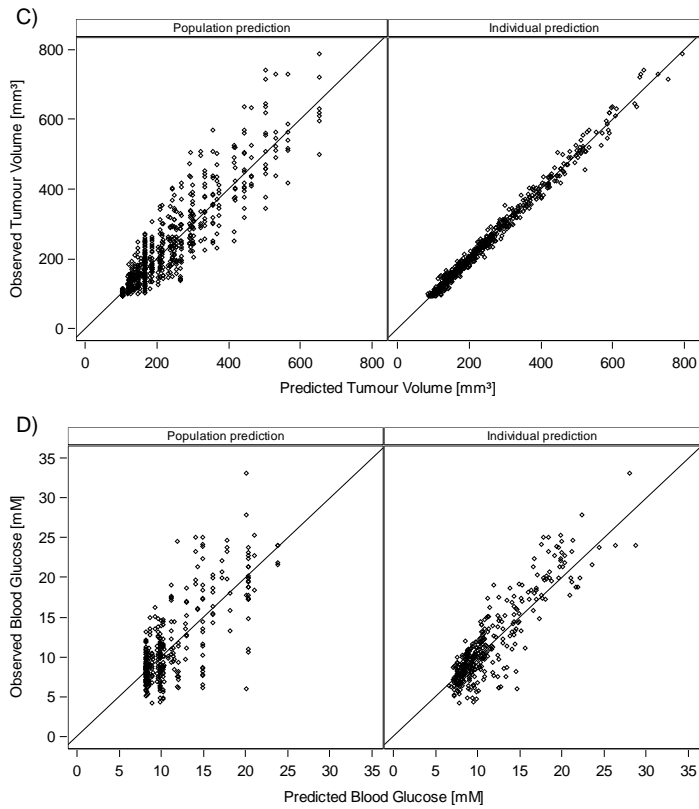
Fig. 1 Observed *vs* population predicted (left panels) and individual predicted (right panels) A) BI 893923 plasma concentrations, B) tumor pIGF1R levels, C) tumor volumes, D) blood glucose concentrations.

Online Resource Material 4: Visual predictive checks
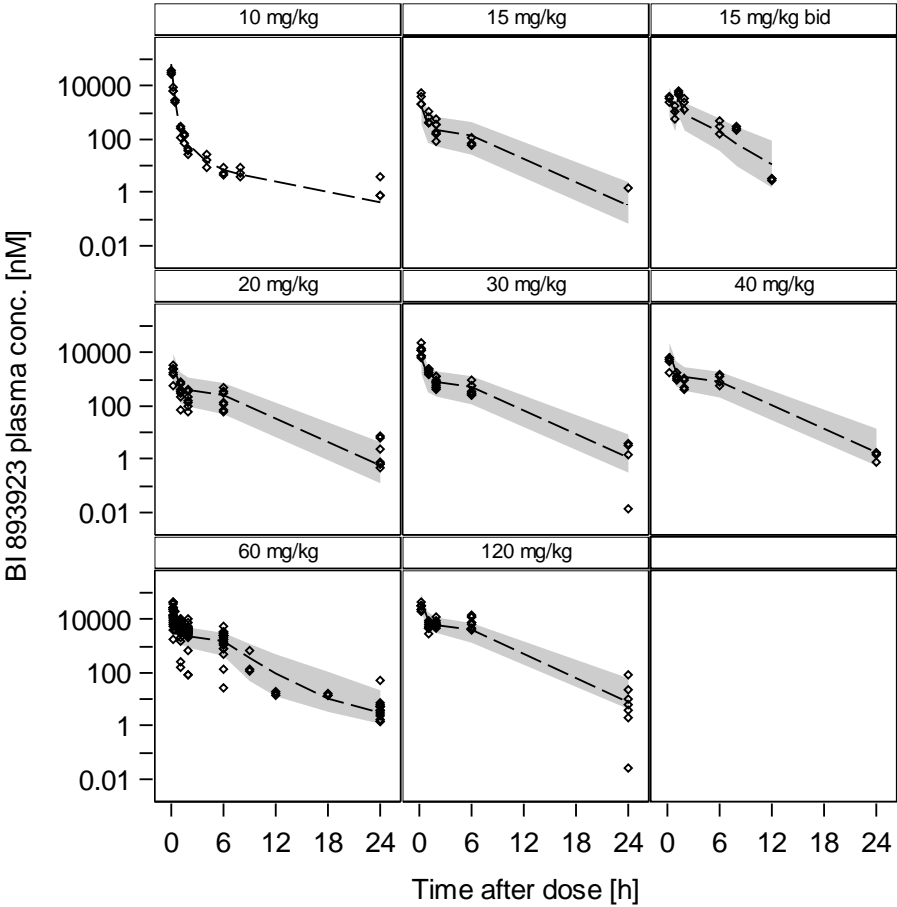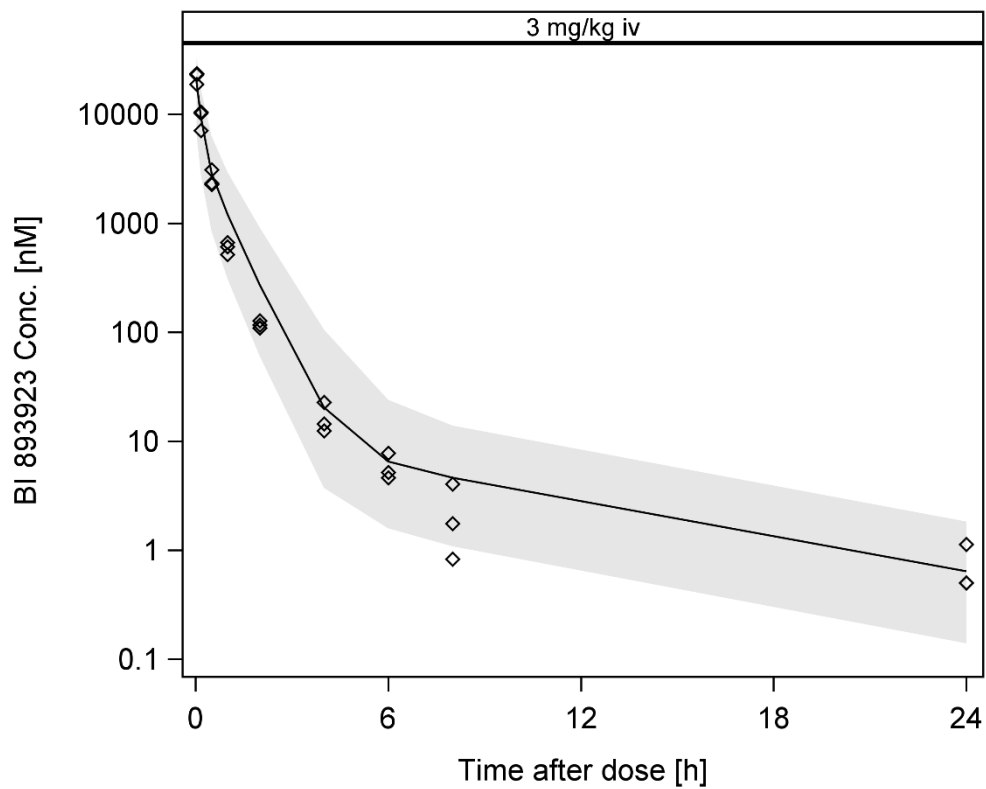

Fig. 1 Visual predictive check for BI 893923 plasma concentration based on 500 simulations: Observed BI 893923 plasma concentration (black diamonds) is compared to median (dashed line) and 90% confidence interval (shaded area) of model predicted concentration.
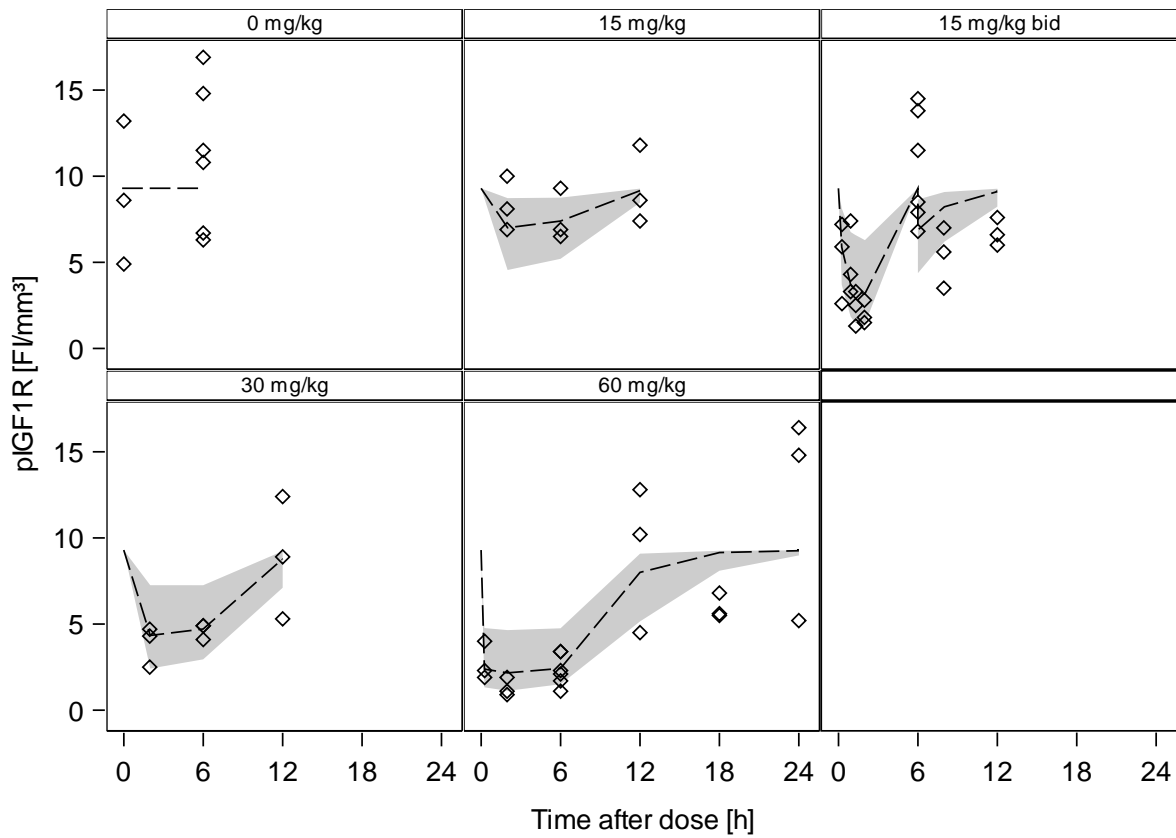
Fig. 2 Visual predictive check for biomarker based on 500 simulations: Observed pIGF1R level (black diamonds) is compared to median (dashed line) and 90% confidence interval (shaded area) of model predicted pIGF1R level.
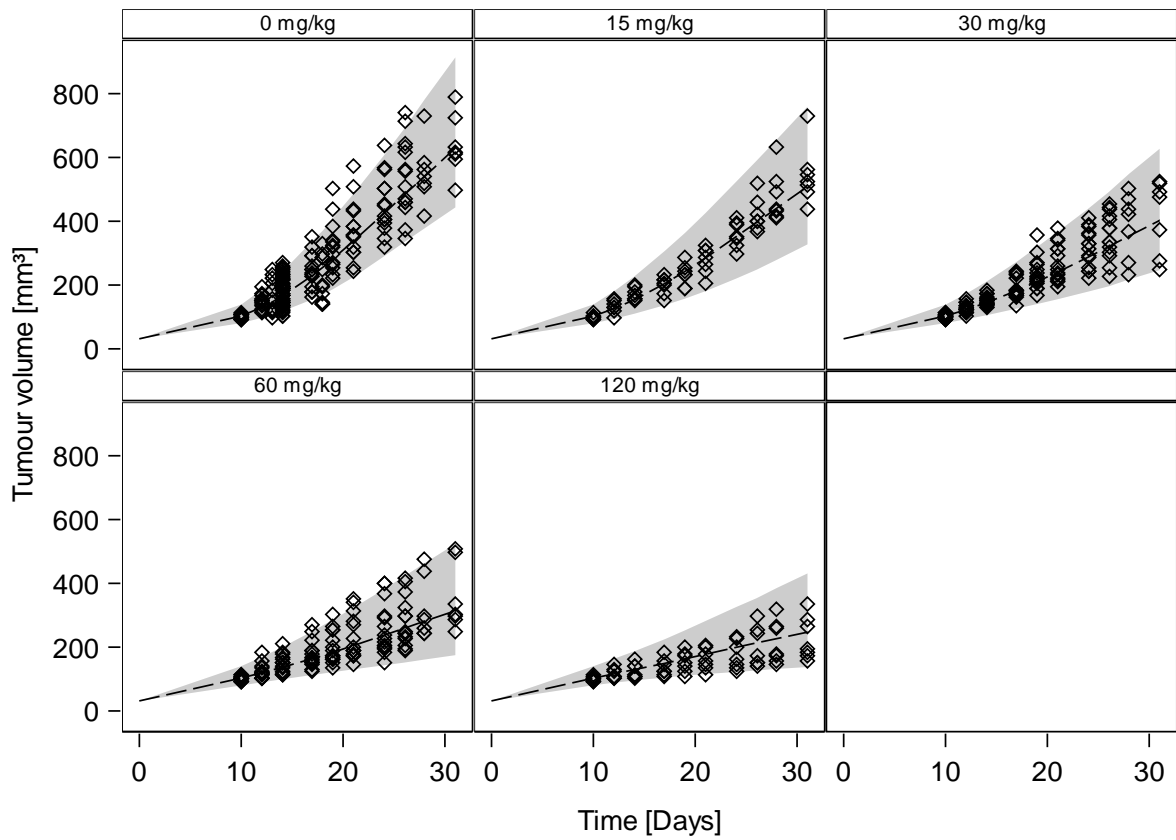
Fig. 3 Visual predictive check for tumor growth based on 500 simulations: Observed tumor volume (black diamonds) is compared to median (dashed line) and 90% confidence interval (shaded area) of model predicted tumor volume.
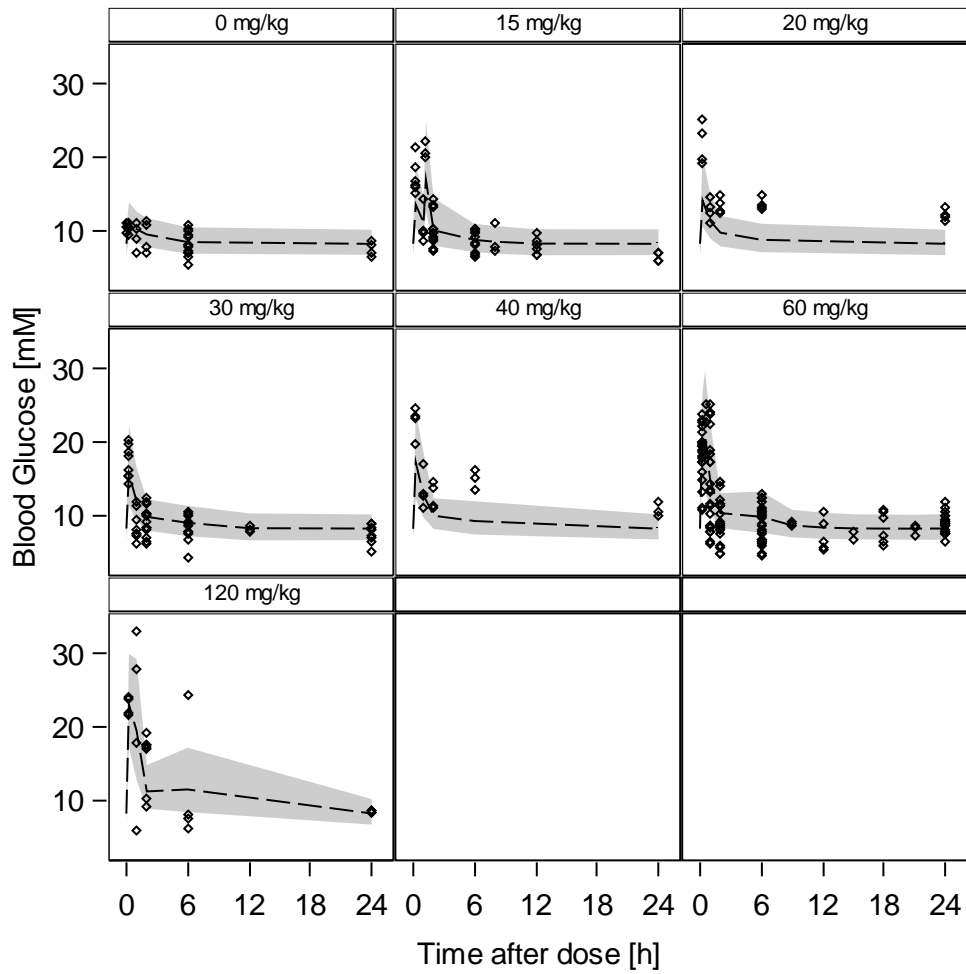
Fig. 4 Visual predictive check for blood glucose based on 500 simulations: Observed blood glucose (black diamonds) is compared to median (dashed line) and 90% confidence interval (shaded area) of model predicted blood glucose.

10.3 Supporting Information III: An allometric pharmacokinetic/pharmacodynamics model for BI 893923, a novel IGF-1 receptor inhibitor

Supplemental Materials to:

An allometric pharmacokinetic/pharmacodynamics model for BI 893923, a novel IGF-1 receptor inhibitor

Melanie I. Titze[1], Otmar Schaaf[2], Marco H. Hofmann[2], Michael P. Sanderson[2], Stephan K. Zahn[2], Jens Quant[2], Thorsten Lehr[1]

[1]Clinical Pharmacy, Saarland University, Saarbrücken, Germany
[2]Boehringer Ingelheim RCV GmbH & Co KG, Vienna, Austria

Online Resource 1: Data characterization for allometric PK modelling

	Number of Animals		Number of Observations				Dose [mg/kg]	
	i.v.	p.o.	i.v.		p.o.		i.v.	p.o.
			> LLOQ	< LLOQ	> LLOQ	< LLOQ		
Mouse	6	9	30	0	32	13	10	20, 60
Rat	3	21	21	3	147	0	5	15, 20, 30, 60, 120
Dog	3	15	24	3	125	10	3	1, 3, 9, 18, 36
Minipig	3	0	25	2	0	0	3	-
Monkey	3	3	26	1	27	0	3	18

LLOQ: Lower limit of quantitation

Online Resource 2: Individual weighted residuals (IWRES) versus population predictions (left panels) and versus time after dose (left panels) for BI 893923 plasma concentration.
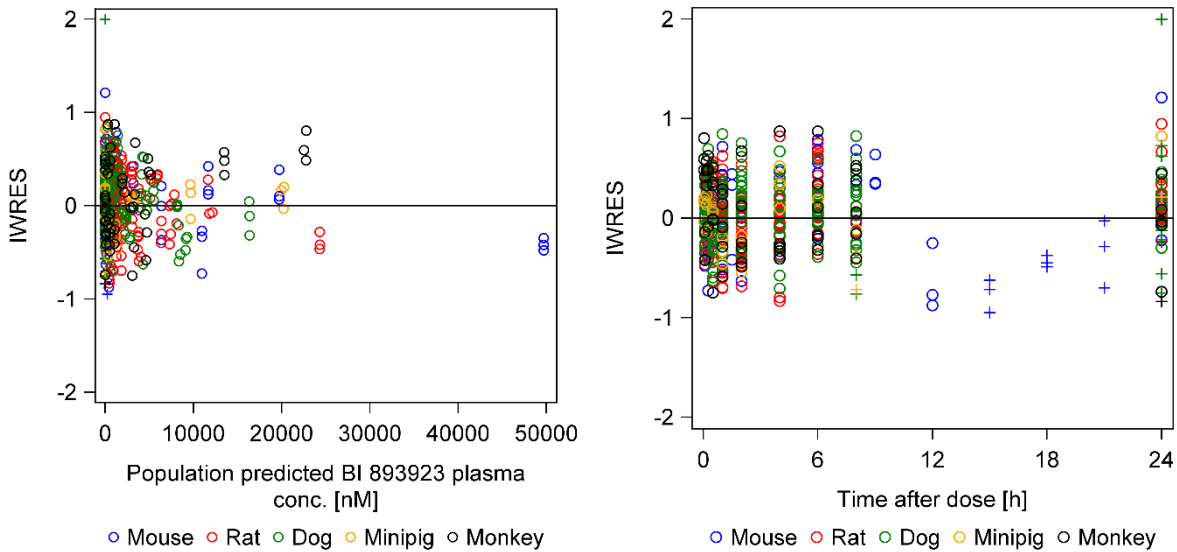
Online Resource 3: Visual predictive checks for allometric PK model
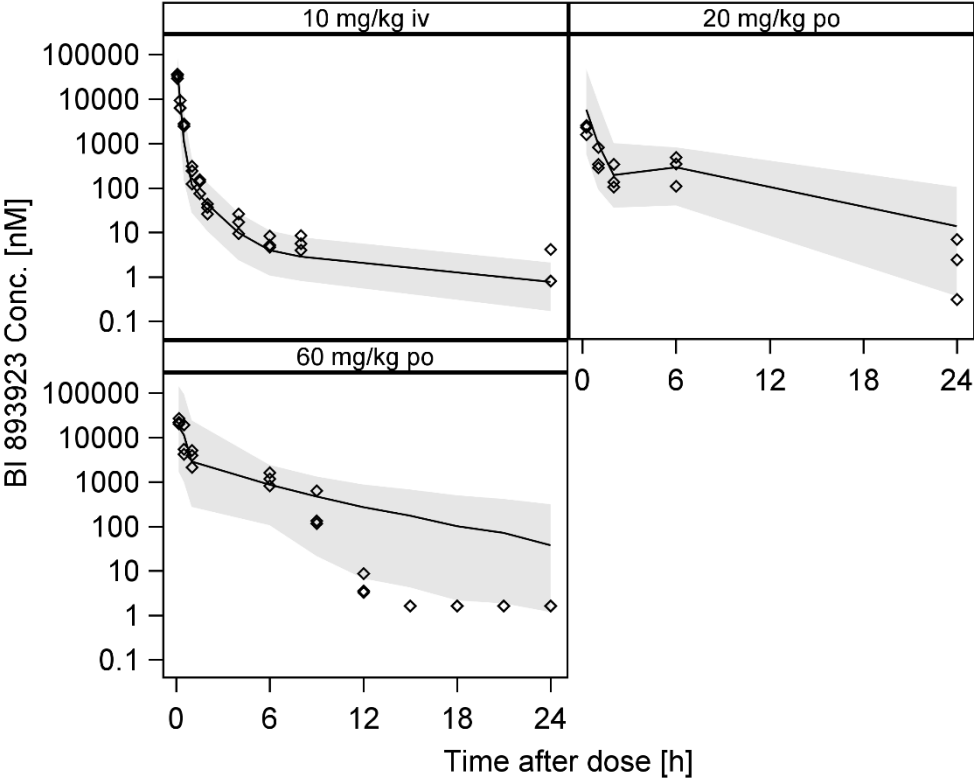
Fig. 1 VPC for mice based on 1000 simulations. Observed BI 893923 plasma concentration (black diamond) is compared to median (solid line) and 90% confidence interval (shaded area) of model predicted concentration.
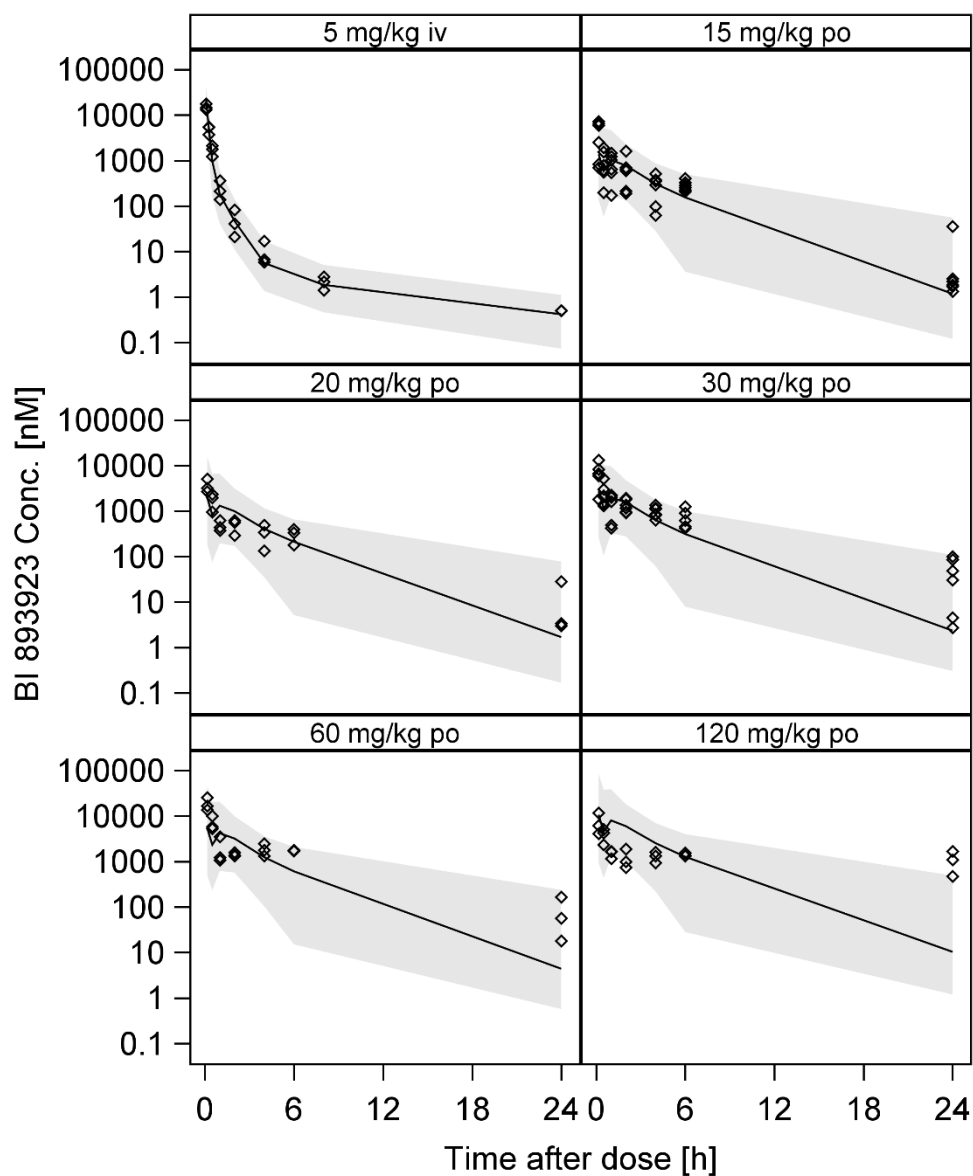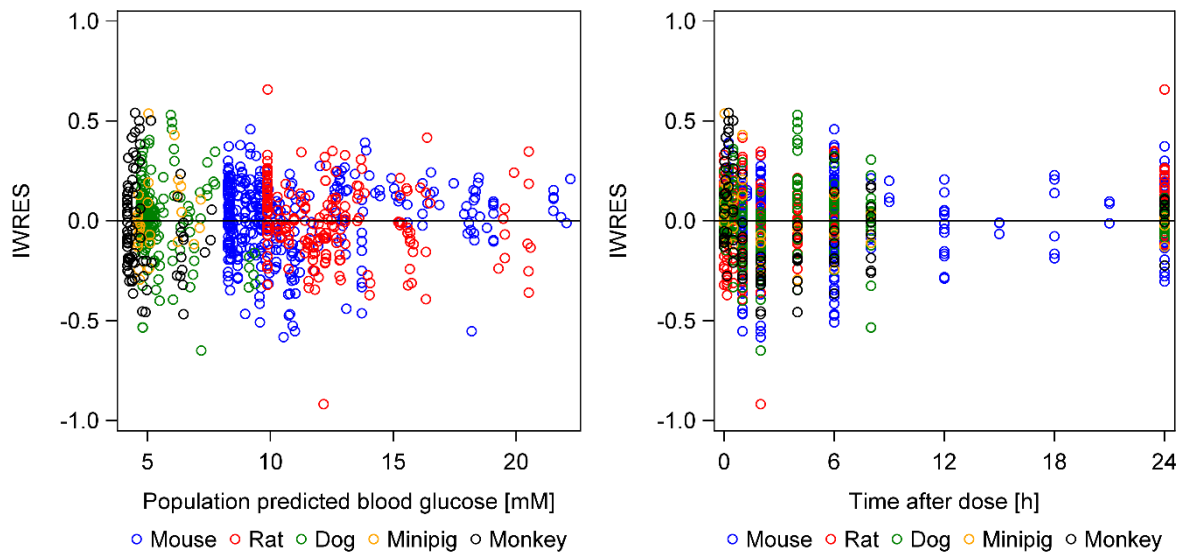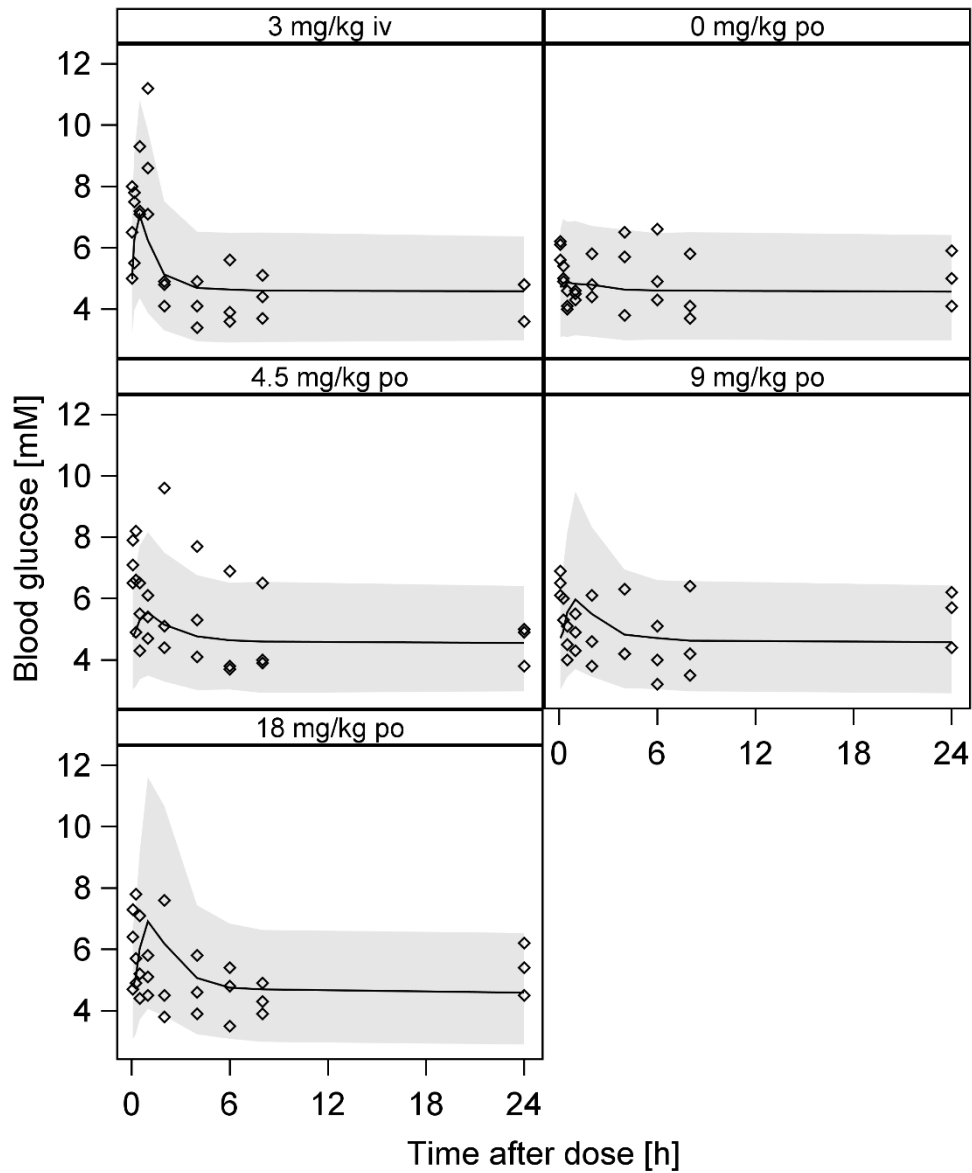
Fig. 2 VPC for rats based on 1000 simulations. Observed BI 893923 plasma concentration (black diamond) is compared to median (solid line) and 90% confidence interval (shaded area) of model predicted concentration.
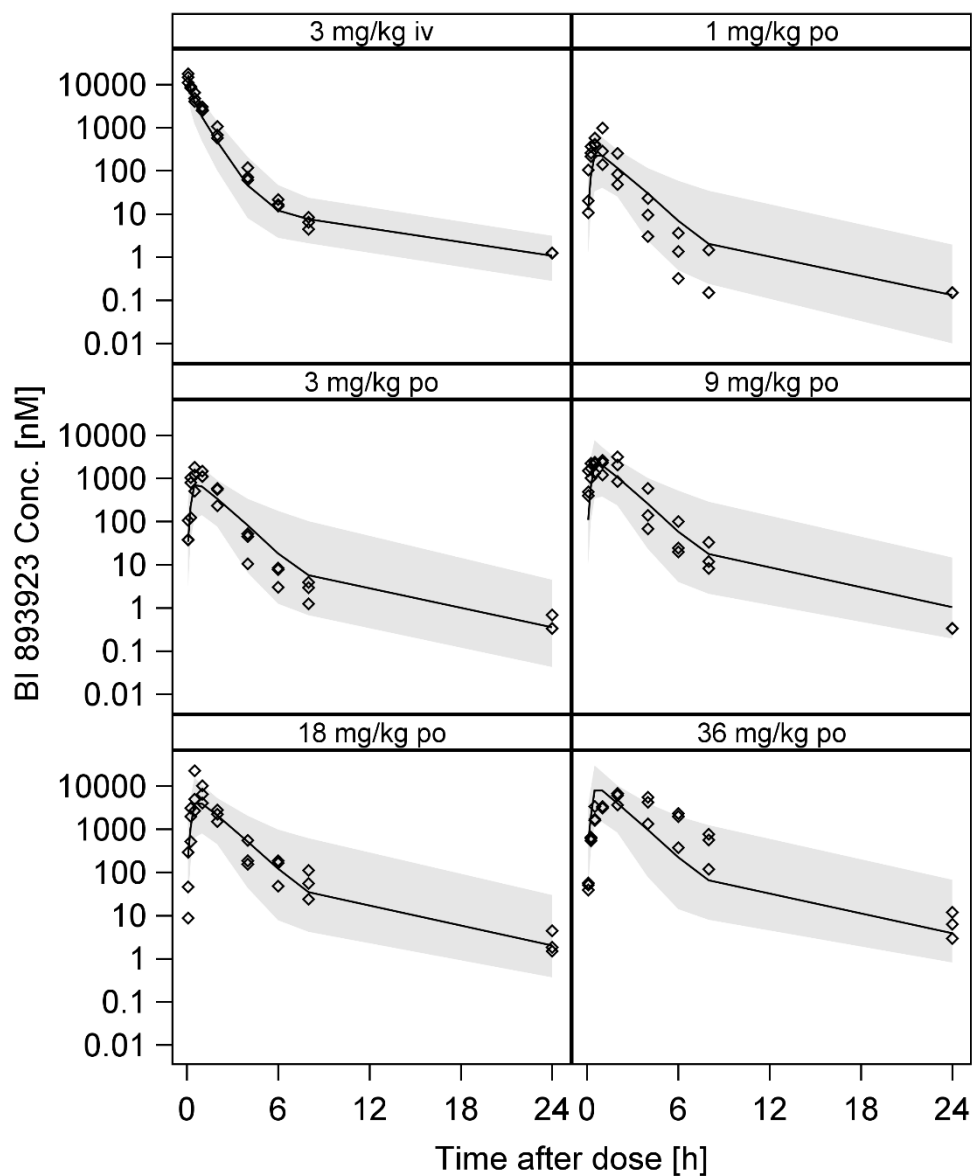
Fig. 3 VPC for dogs based on 1000 simulations. Observed BI 893923 plasma concentration (black diamond) is compared to median (solid line) and 90% confidence interval (shaded area) of model predicted concentration.

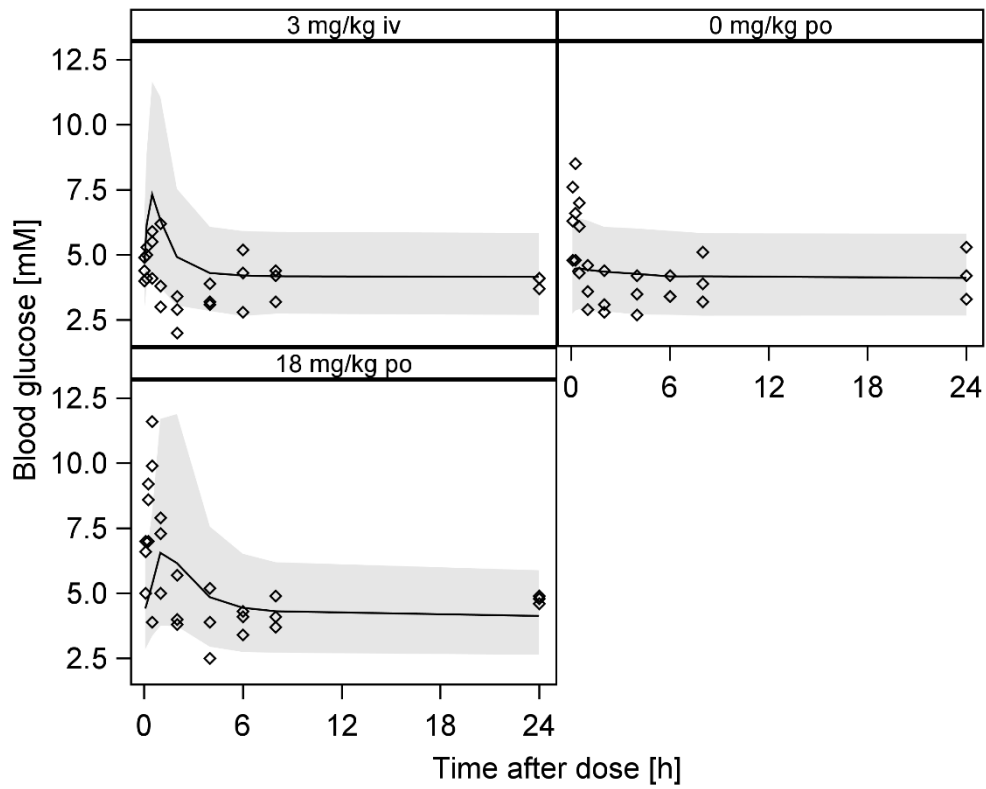**Fig. 4** VPC for minipigs based on 1000 simulations. Observed BI 893923 plasma concentration (black diamond) is compared to median (solid line) and 90% confidence interval (shaded area) of model predicted concentration.
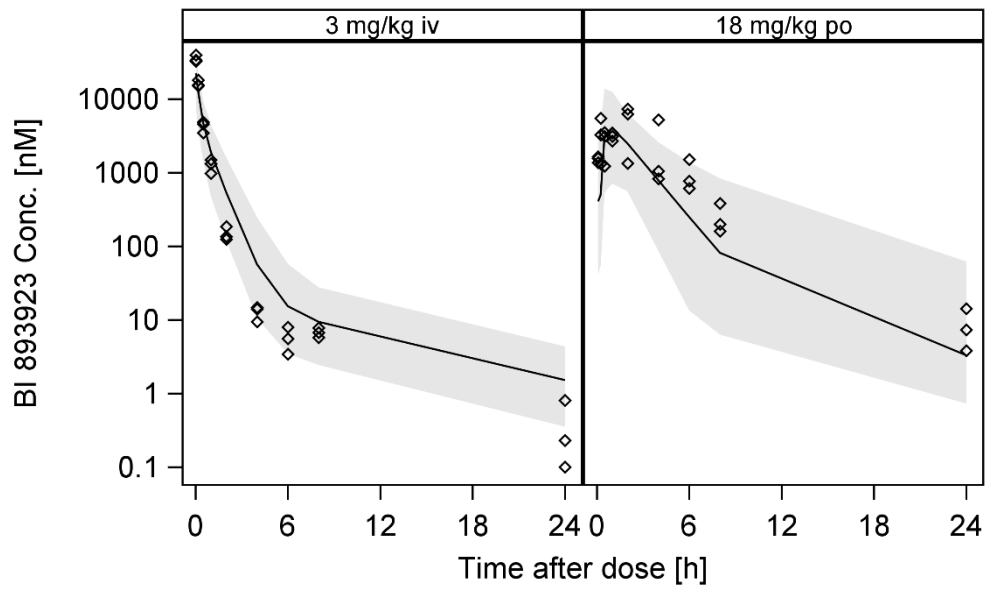
Fig. 5 VPC for monkeys based on 1000 simulations. Observed BI 893923 plasma concentration (black diamond) is compared to median (solid line) and 90% confidence interval (shaded area) of model predicted concentration.

Online Resource 4: Data characterization for allometric glucose modelling

	Number of Animals		Number of Observations		Dose [mg/kg]	
	i.v.	p.o.	i.v.	p.o.	i.v.	p.o.
Mouse	-	136	-	347	-	0, 15, 20, 30, 40, 60, 120
Rat	-	24	-	192		15, 20, 30, 60, 120
Dog	3	18	30	180	3	0, 1, 3, 9, 18, 36
Minipig	3	12	30	120	3	0, 4.5, 9, 18
Monkey	3	6	30	60	3	0, 18

Online Resource 5: Individual weighted residuals (IWRES) versus population predictions (left panels) and versus time after dose (left panels) for blood glucose.

Online Resource 6: Visual predictive checks for allometric PK/PD model
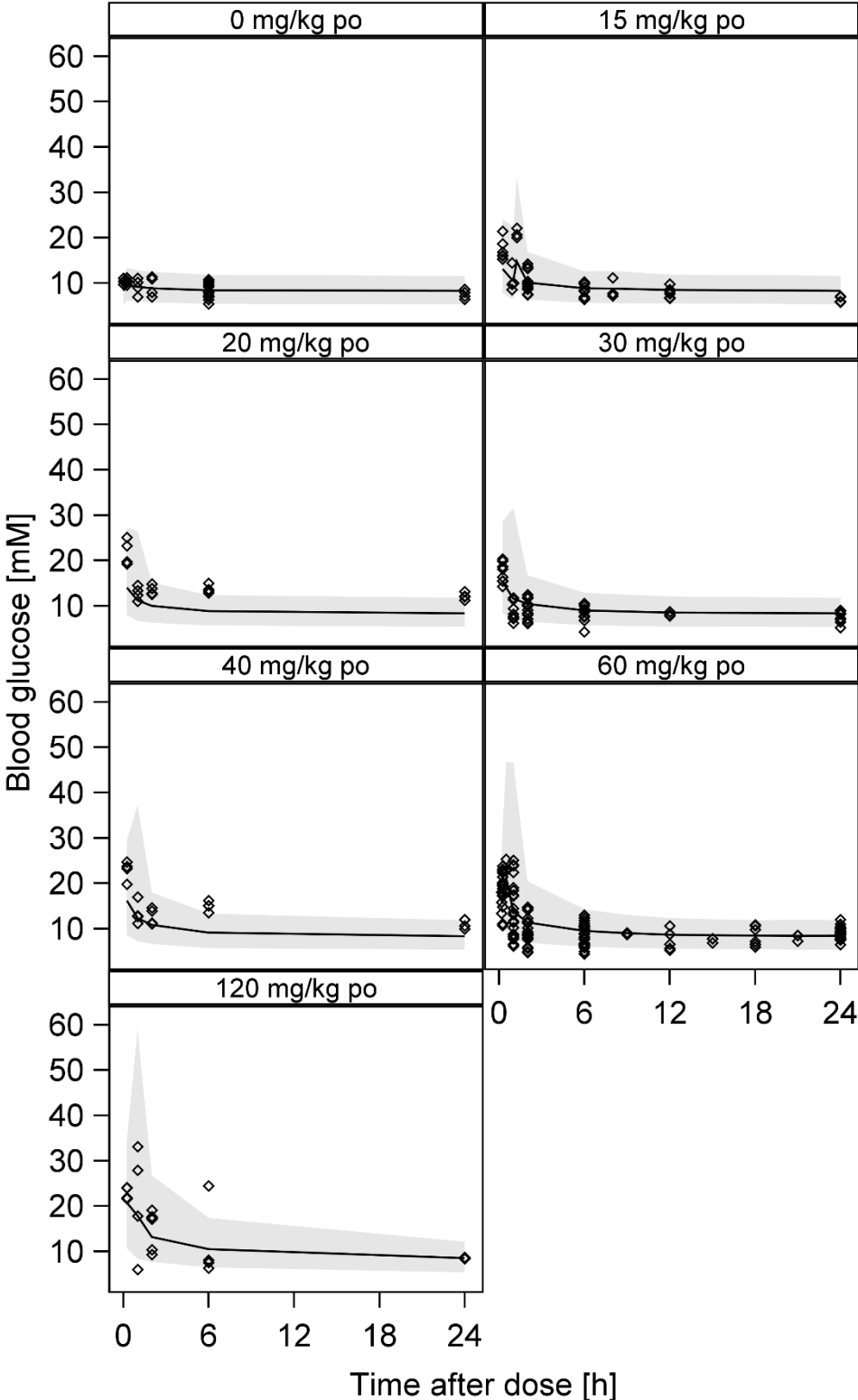
Fig. 1 VPC for mice based on 1000 simulations. Observed blood glucose (black diamond) is compared to median (solid line) and 90% confidence interval (shaded area) of model predicted blood glucose.
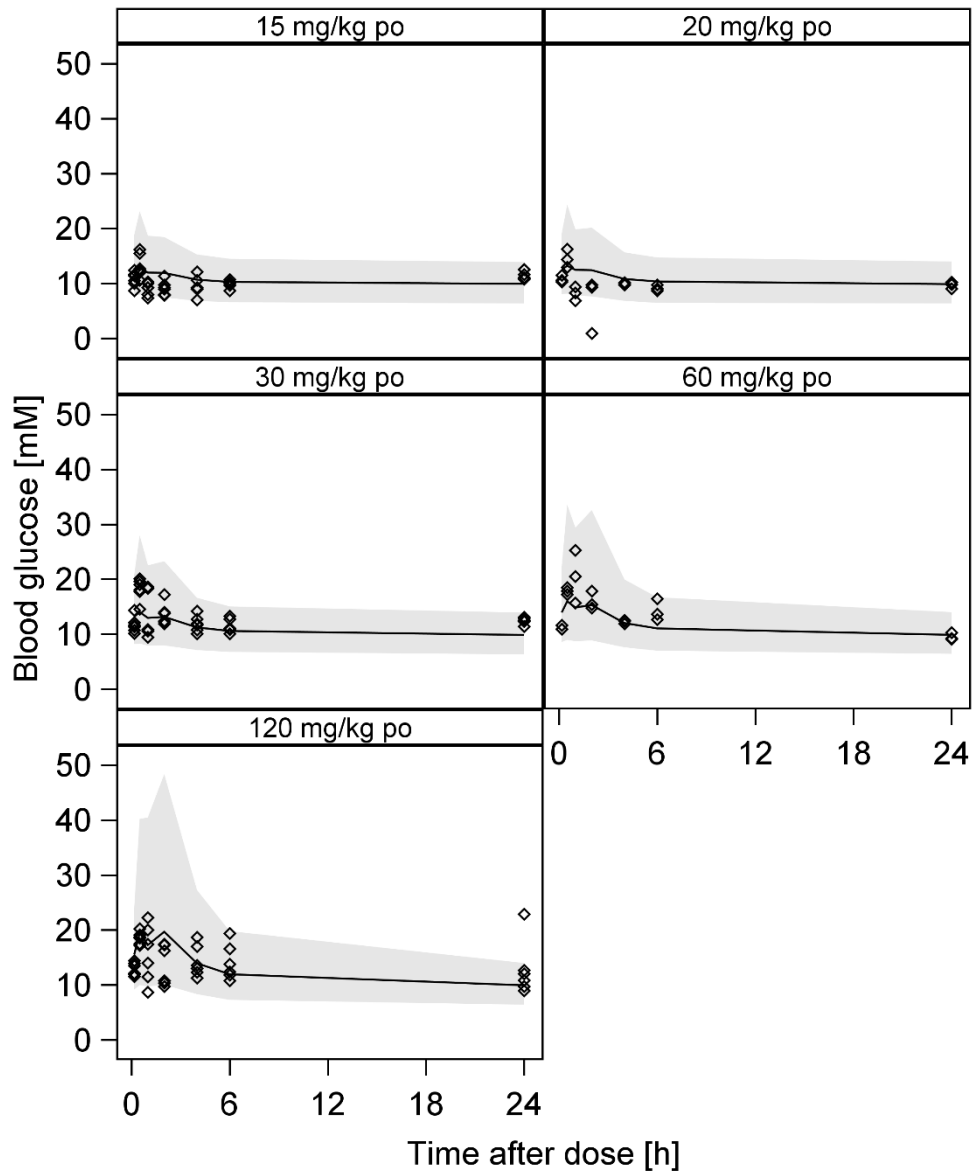
Fig. 2 VPC for rats based on 1000 simulations. Observed blood glucose (black diamond) is compared to median (solid line) and 90% confidence interval (shaded area) of model predicted blood glucose.
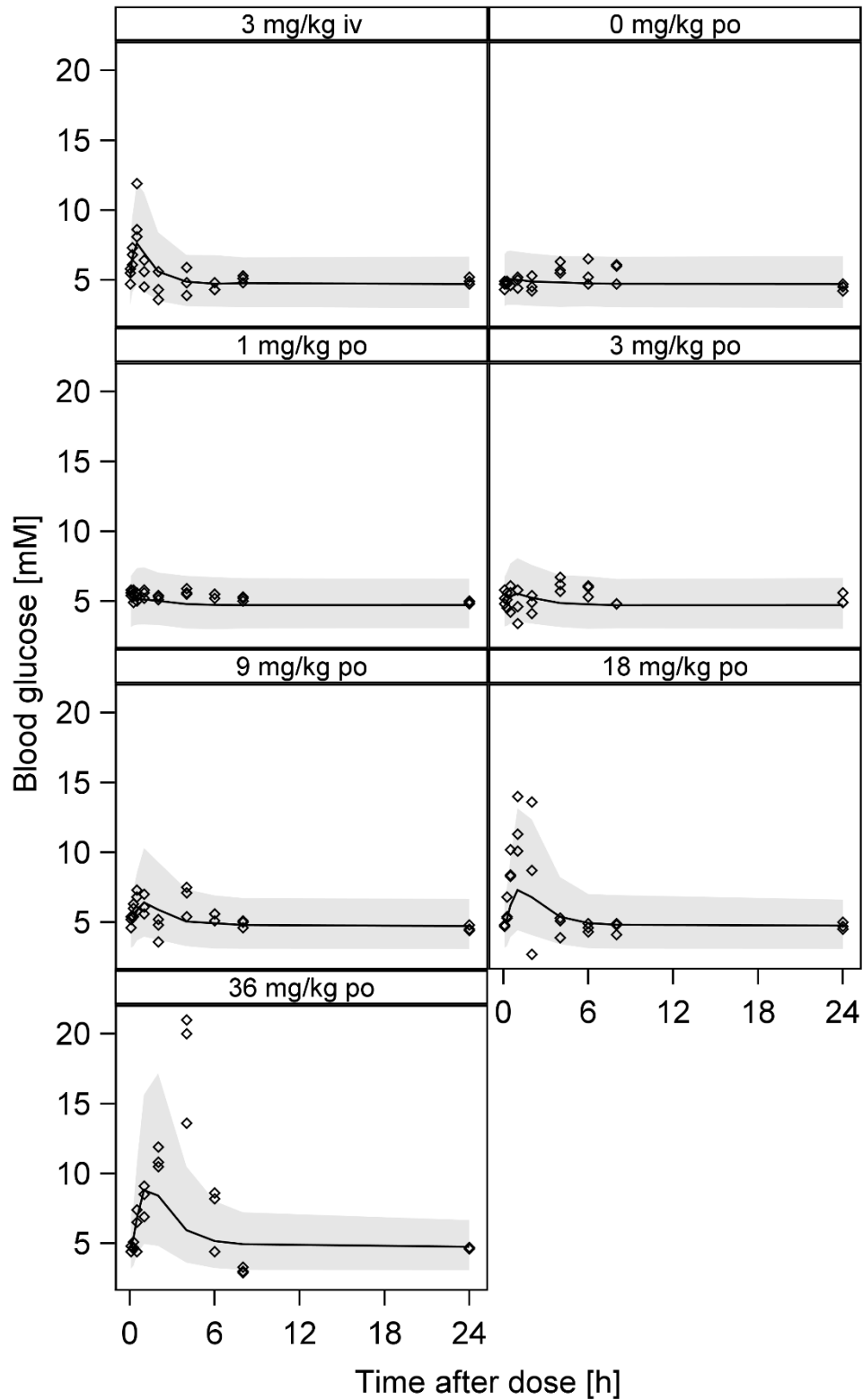
Fig. 3 VPC for dogs based on 1000 simulations. Observed blood glucose (black diamond) is compared to median (solid line) and 90% confidence interval (shaded area) of model predicted blood glucose.

Fig. 4 VPC for minipigs based on 1000 simulations. Observed blood glucose (black diamond) is compared to median (solid line) and 90% confidence interval (shaded area) of model predicted blood glucose.

Fig. 5 VPC for monkeys based on 1000 simulations. Observed blood glucose (black diamond) is compared to median (solid line) and 90% confidence interval (shaded area) of model predicted blood glucose.

Online Resource 7: Model control stream

```
$PROBLEM allometric scaling of PK/PD

$INPUT SPECIES ID DAY TIME TAD AMT DOSE DV MDV EVID DGR CMT LLOQ BLQ BW BRAIN
FLAG
$SUBROUTINES ADVAN6

$MODEL
NCOMPS = 13
COMP = (DEPOT1)          ; Depot 1
COMP = (DEPOT2)          ; Depot 2
COMP = (CENTRAL)         ; Central PK comp.
COMP = (PERI1)           ; Peripheral PK comp. 1
COMP = (PERI2)           ; Peripheral PK comp. 2
COMP = (BIOM)            ; Biomarker
COMP = (EFFECT)          ; Biophase
COMP = (TUMOR)           ; Tumor
COMP = (TRANS1)          ; Biomarker transit comp. 1
COMP = (TRANS2)          ; Biomarker transit comp. 1
COMP = (GLUCOSE)         ; Glucose comp.
COMP = (PLAC_C)          ; Central Placebo comp.
COMP = (PLAC_P)          ; Peripheral Placebo comp;


$PK
;PK MODEL
;body and brain weight [g] -> convert to kg
CL    = THETA(1) *(BW/1000)**THETA(7)*(BRAIN/1000)**THETA(13) *EXP(ETA(3))
V3    = THETA(2) *(BW/1000)**THETA(8)
Q4    = THETA(3) *(BW/1000)**THETA(9)
V4    = THETA(4) *(BW/1000)**THETA(10)
Q5    = THETA(5) *(BW/1000)**THETA(11)
V5    = THETA(6) *(BW/1000)**THETA(12)

;oral parameters
KA1   = THETA(14) *(BW/1000)**THETA(15)
KA2   = THETA(16) *(BW/1000)**THETA(17) *EXP(ETA(4))
ALAG2 = THETA(18) *(BW/1000)**THETA(19)
F1    = THETA(20) *(BW/1000)**THETA(21) *EXP(ETA(1))
F2    = THETA(22) *(BW/1000)**THETA(23) *EXP(ETA(2))
FTOT  = F1+F2              ; total bioavailability

K34   = Q4/V3
K43   = Q4/V4
K35   = Q5/V3
K53   = Q5/V5
KE    = CL/V3
S3    = V3

; BIOMARKER
BWR   = (BW/1000)/0.02        ; body weight ratio = (BW species)/(mean BW mouse)

KDEPHOS = THETA(24) * BWR**(-0.25)      ; IGF1R dephosphorylation rate
IC50    = THETA(25)
BMNUL   = THETA(26)                     ; baseline level of pIGF1R
A_0(6)  = BMNUL
KPHOS   = KDEPHOS * BMNUL               ; IGF1R phosphorylation rate
K1      = THETA(27) *(BW/1000)**0.222   ; rate const. for distribution in tumor
                              ; 0.222 is the mean of KA1 and KA2 exponents

; TUMOR
L0_1  = THETA(28) * BWR**(-0.25) * EXP(ETA(5))  ; exponential growth rate
L1_1  = THETA(29) * BWR**(-0.25) * EXP(ETA(6))  ; linear growth rate
Z     = 20
BASE  = THETA(30)                               ; tumor volume baseline
A_0(8) = BASE

K2    = THETA(31) *(BW/1000)**0.222 * EXP(ETA(7)); transit rate for biomarker
                                        ; inhibition
```

67

```
                                                      ; 0.222 is the mean of KA1
                                                      ; and KA2 exponents
A_0(9) = 1   ; baseline transit 1
A_0(10)= 1   ; baseline transit 2
; GLUCOSE
KDISP  = THETA(32) * BWR**(THETA(36))              ; glucose disposal rate

;blood glucose baselines [mMol/l]
IF(SPECIES.EQ.1) BL = THETA(33) * EXP(ETA(8))   ; MOUSE
IF(SPECIES.EQ.2) BL = THETA(34) * EXP(ETA(8))   ; RAT
IF(SPECIES.EQ.3) BL = THETA(35) * EXP(ETA(8))   ; DOG
IF(SPECIES.EQ.4) BL = THETA(36) * EXP(ETA(8))   ; MONKEY
IF(SPECIES.EQ.5) BL = THETA(37) * EXP(ETA(8))   ; PIG
A_0(11)= BL

KSYN   = KDISP * BL                                ; glucose synthesis rate
EMAX   = THETA(38)
EC50   = THETA(39) * EXP(ETA(9))

;PLACEBO MODEL
F13    = THETA(40) * BWR**(THETA(41))              ; placebo effect

;values from Derendorf et al. J Clin Pharmacol 1991;31:473-6
V7     = 429.44  * ((BW/1000)/74)**0.75
V8     = 348.3   * ((BW/1000)/74)**0.75
CL7    = 356.57  * ((BW/1000)/74)**0.75
CL8    = 2445.17 * ((BW/1000)/74)**0.75

K70    = CL7/V7
K78    = CL8/V7
K87    = CL8/V8

$DES
C3  = A(3)/V3                  ; concentration central PK compartment
CE  = A(7)                     ; effect compartment

EFF = CE/(IC50 + CE)           ; drug effect on biomarker
INH = A(6)/BMNUL               ; direct tumor inhibition
SUM = INH * A(9) * A(10)        ; time-delayed tumor inhibition

L1 = L1_1 * SUM                ; decreased linear growth rate
L0 = L0_1 * SUM                ; decreased exponential growth rate

EFF2 = (EMAX*C3)/(EC50+C3)     ; drug effect on glucose
PLAC = A(13)                   ; placebo effect

; PK
DADT(1)  = -KA1*A(1)
DADT(2)  = -KA2*A(2)
DADT(3)  =  KA1*A(1)+KA2*A(2)-KE*A(3)-K34*A(3)+K43*A(4)-K35*A(3)+K53*A(5)
DADT(4)  =                       K34*A(3)-K43*A(4)
DADT(5)  =                                          K35*A(3)-K53*A(5)
; BIOMARKER
DADT(6)  = KPHOS * (1-EFF) - KDEPHOS*A(6)
DADT(7)  = K1*C3 - K1*A(7)
; TUMOR
DADT(8)  = (L0*A(8))/((1+((L0/L1)*A(8))**Z)**(1/Z))
DADT(9)  = K2*INH - K2*A(9)
DADT(10) = K2*A(9) - K2*A(10)
; GLUCOSE
DADT(11) = KSYN * (1+PLAC) - KDISP *A(11) * (1-EFF2)
DADT(12) = -K78*A(12) + K87*A(13) - K70*A(12)
DADT(13) =  K78*A(12) - K87*A(13)


$ERROR
IPRED = A(3)/V3
IF(CMT.EQ.6)  IPRED = A(6)
IF(CMT.EQ.8)  IPRED = A(8)
IF(CMT.EQ.11) IPRED = A(11)
DEL = 0
```

68

```
IF(IPRED.EQ.0) DEL = 0.0001
W = IPRED
IRES  = DV - IPRED
IWRES = IRES/(W+DEL)
Y = IPRED + W*EPS(1) + EPS(2)
IF(CMT.EQ.6)  Y = IPRED + W*EPS(3)
IF(CMT.EQ.8)  Y = IPRED + W*EPS(4) + EPS(5)
IF(CMT.EQ.11) Y = IPRED + W*EPS(6)
```

Online Resource 8: Maximum achievable human net clinical benefit with associated tumor growth inhibition (TGI) and duration of hyperglycemia within one day (T_{HG}) for different dosing regiments after 90 days of daily dosing

| Regiment	Daily Dose [mg]	max. NCB	TGI [%]	T_{HG} [h]
SD	5000	66.4	73.9	7.5
BID 6 h	5000	80	87.2	7.2
BID 9 h	5000	82.6	89.6	7
BID 12 h	5000	82.9	89.9	7
TID	2750	90.4	90.4	0

Online Resource 9: Sensitivity analysis for BI 893923 plasma concentration (Fig. 1), pIGF1R modulation (Fig. 2), tumor growth inhibition (Fig. 3) and blood glucose level (Fig. 4) in humans after single oral dose of 2000 mg. Every parameter was changed in a range of 0.2 x parameter to 5 x parameter.
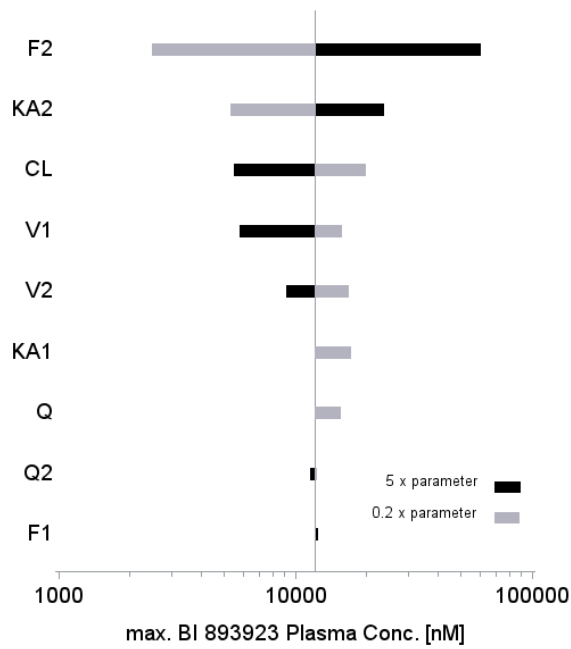
Fig. 1 BI 893923 plasma concentration
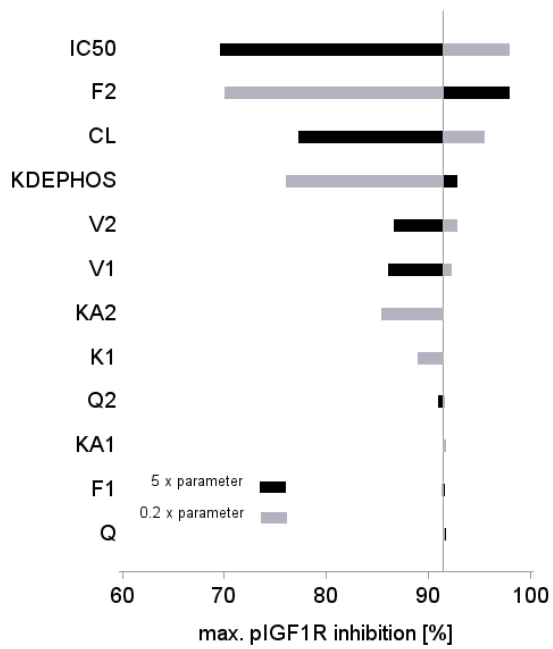
Fig. 2 pIGF1R inhibition
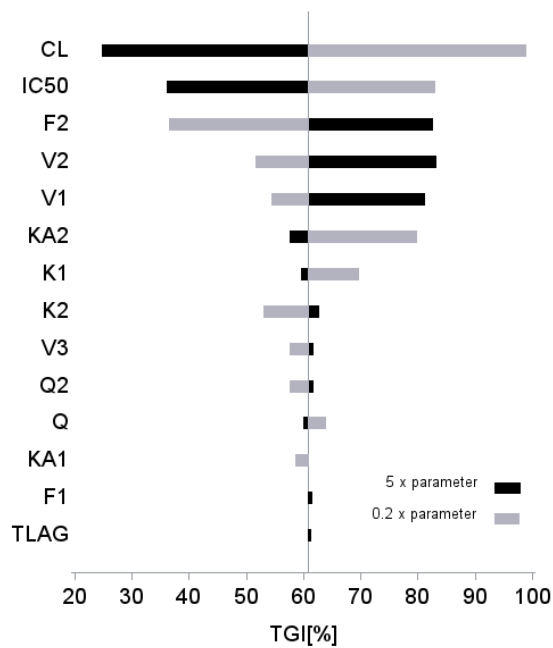
Fig. 3 Tumor growth inhibition
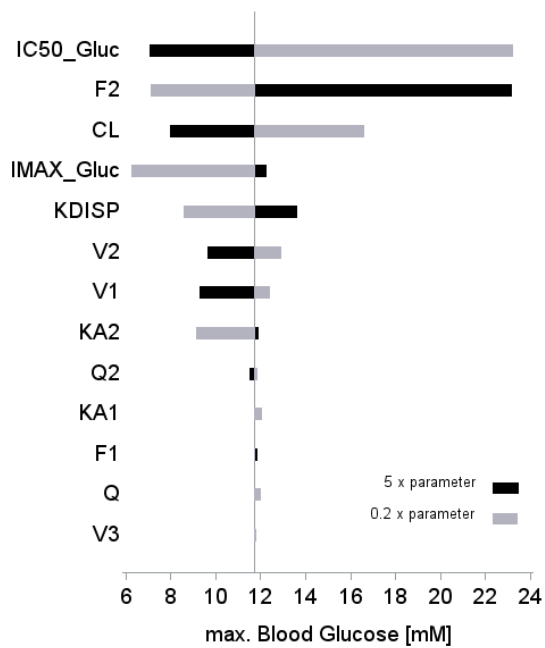
Fig. 4 Blood Glucose

For maximum pIGF1R inhibition a decrease of the receptor dephosphorylation rate leads to a markedly reduction in pIGF1R inhibition whereas an increase of the parameter results in less increased receptor inhibition, since already more than 90% of receptor are inhibited with the baseline parameter value. Despite to PK parameters, tumor growth inhibition was most sensitive to the concentration in the biophase for half-maximum phosphorylation inhibition of IGF1R (IC_{50}) and to rates for distribution in the tumor (K_1) and transit of biomarker inhibition (K_2). Interestingly, changes in tumor growth rates have no significant impact on the tumor growth inhibition indicating that BI 893923 would affect both fast and slow growing tumors. The level of hyperglycemia was effected most by plasma concentration for half-maximum glucose disposal inhibition ($IC_{50}Gluc$), the maximum inhibition of glucose disposal inhibition ($I_{max}Gluc$) and the glucose disposal rate (K_{DISP}).

Online Resource 10: Sensitivity analysis on input data for BI 893923 plasma concentration (Fig. 1), pIGF1R modulation (Fig. 2), tumor growth inhibition (Fig. 3) and blood glucose level (Fig. 4) in humans after single oral dose of 2000 mg. The predicted outcome for the exclusion of a certain species is compared to prediction based all species.
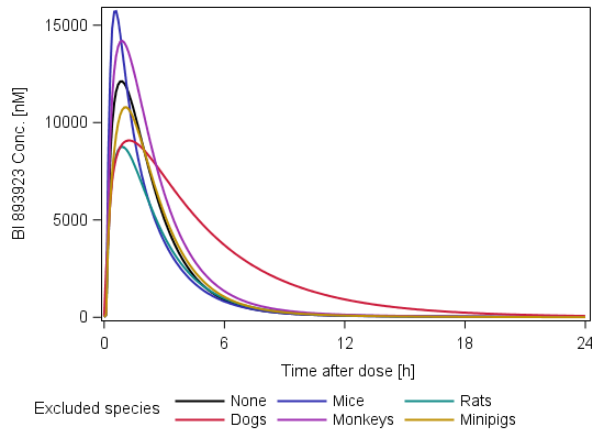
Fig. 1 BI 893923 plasma concentration
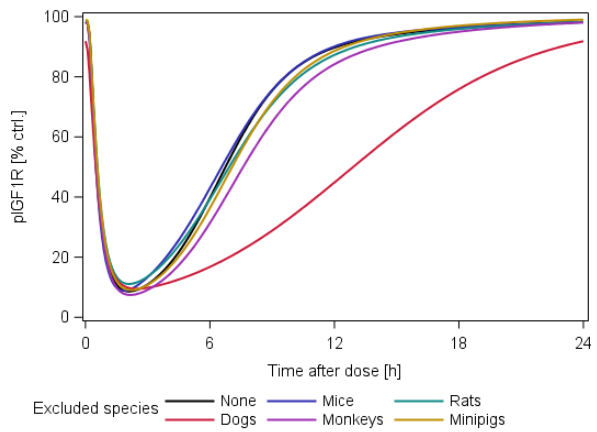
Fig. 2 p-IGF1R level as percentage of control
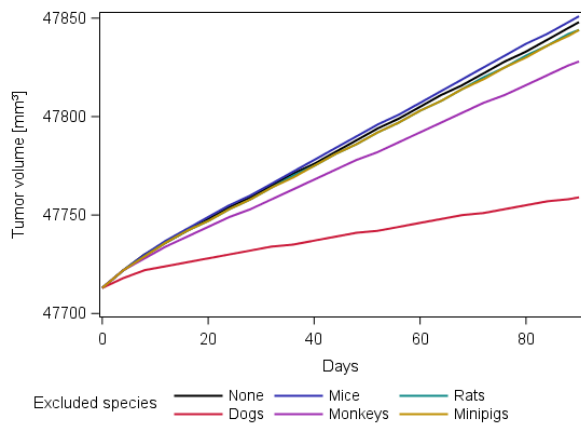
Fig. 3 Tumor volume
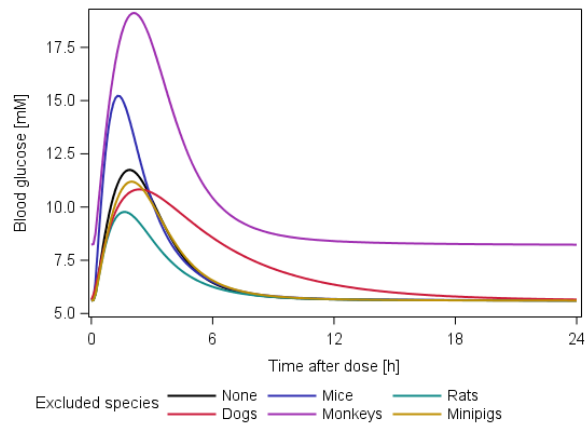
Fig. 4 Blood glucose

Online Resource 11: Simulation of PK/PD relation in human after single oral dose (upper panels) and three times daily dosing (lower panels). Based on 1000 simulations the population median (solid line) and the 90% prediction intervals are plotted for daily doses of 1000, 2000 and 4000mg.
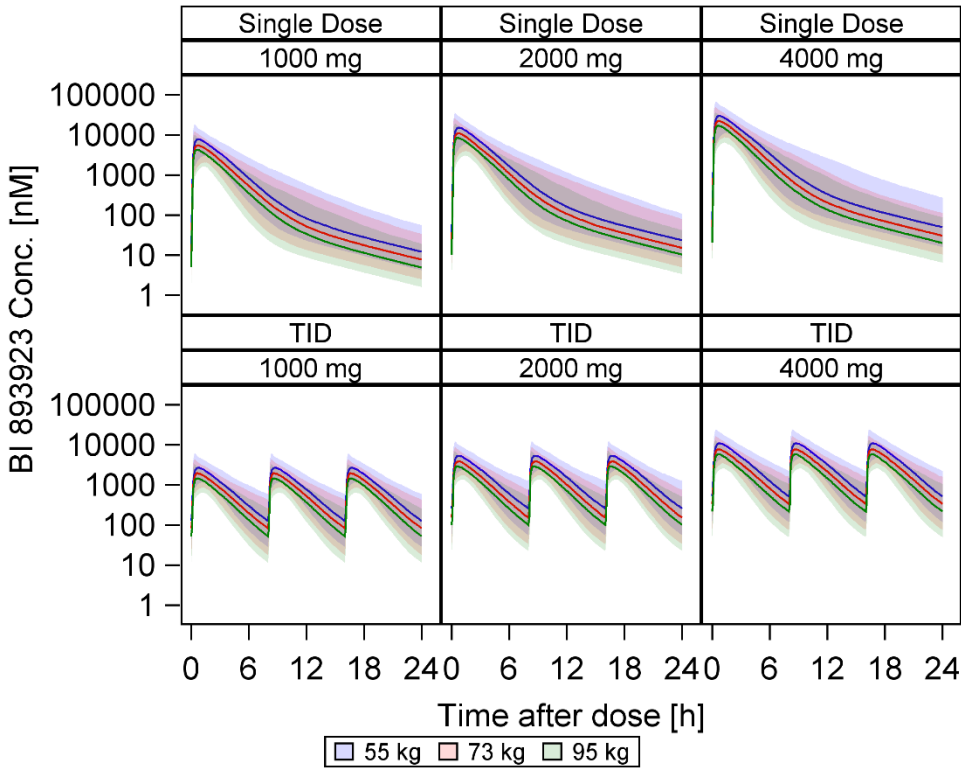
Fig. 1 BI 893923 plasma concentration
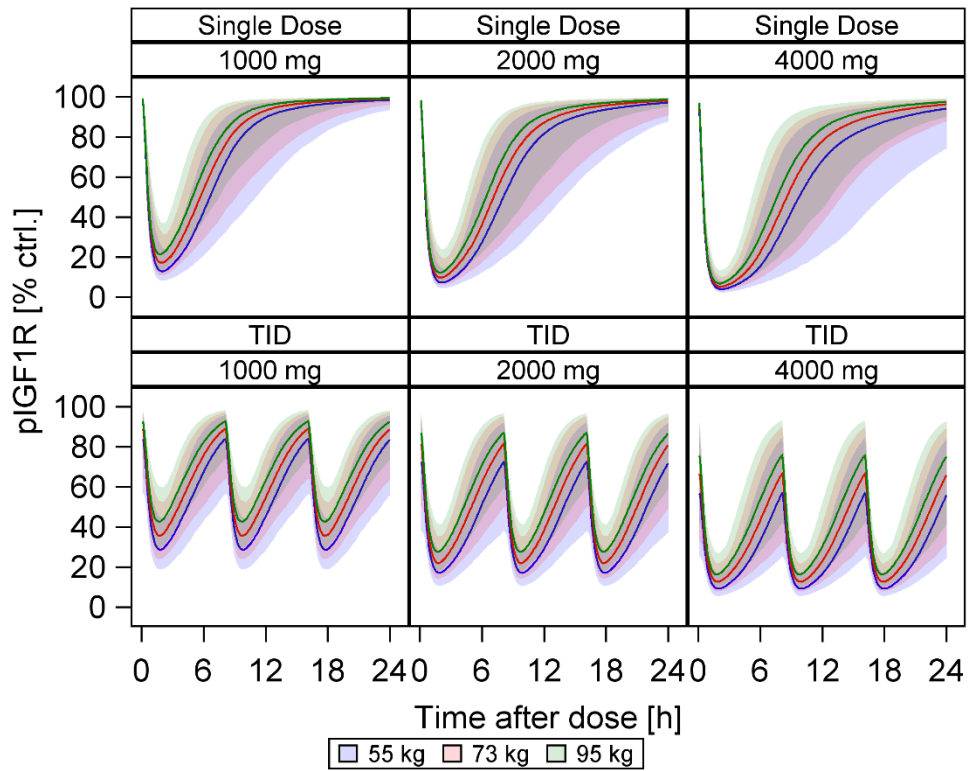
Fig. 2 phospho-IGF1R level as percentage of control
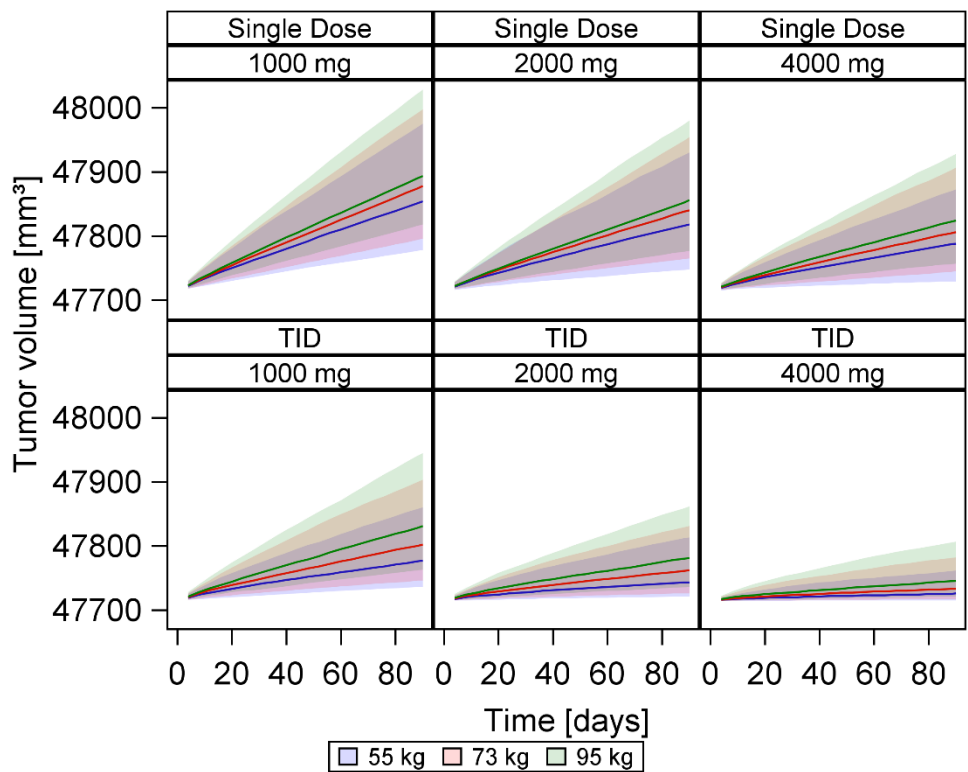
Fig. 3 Tumor volume
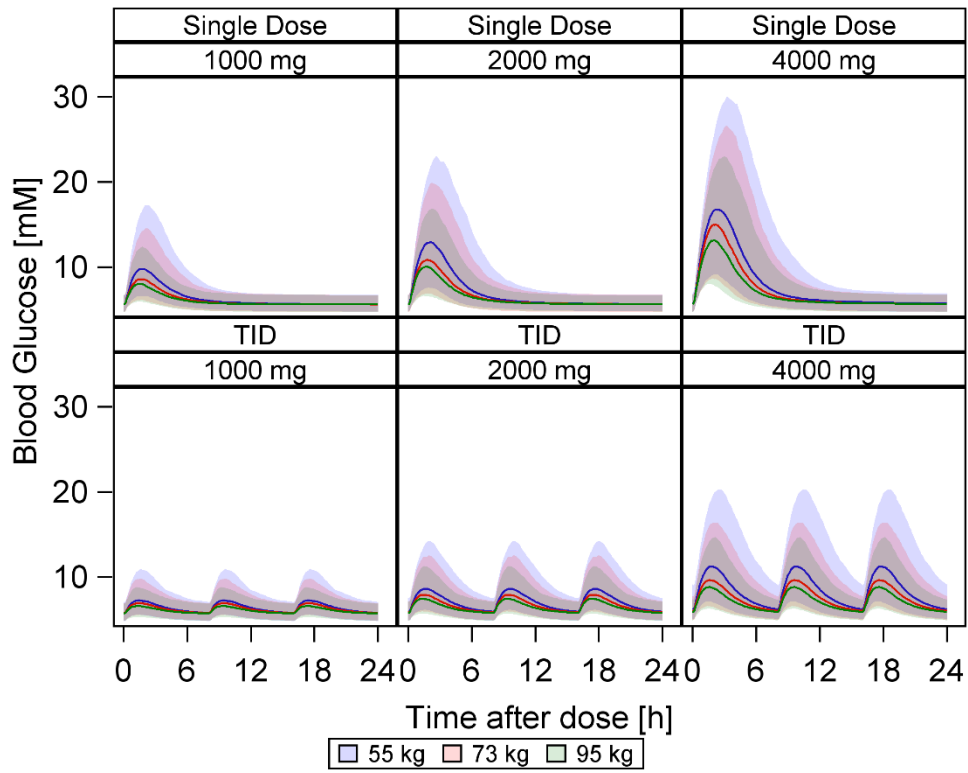
Fig. 4 Blood glucose

11 Appendix

11.1 Original publications

M.I. Titze, J. Frank, M. Ehrhardt, S. Smola, N. Graf, T. Lehr.
A generic viral dynamic model to systematically characterize the interaction between oncolytic virus kinetics and tumor growth.
Eur J Pharm Sci, 97: 38–46 (2017)

M.I. Titze, O. Schaaf, M.H. Hofmann, M.P. Sanderson, S.K. Zahn, J. Quant, T. Lehr.
A comprehensive pharmacokinetic/pharmacodynamics analysis of the novel IGF1R/INSR inhibitor BI 893923 applying in vitro, in vivo and in silico modeling techniques.
Cancer Chemother Pharmacol, 77: 1303–1314 (2016)

M.I. Titze, O. Schaaf, M.H. Hofmann, M.P. Sanderson, S.K. Zahn, J. Quant, T. Lehr.
An allometric pharmacokinetic/pharmacodynamics model for BI 893923, a novel IGF-1 receptor inhibitor.
Cancer Chemother Pharmacol, 79: 545–558 (2017)

11.2 Conference abstracts

M.I. Titze, M. Ehrhardt, S. Smola, N. Graf, T. Lehr.
A semi-mechanistic mathematical model to describe the effect of oncolytic reovirus on in vitro tumor cell growth of U87-glioblastoma cells.
Annual meeting of the German Pharmaceutical Society (DPhG), Freiburg, Germany, 2013.

I. Schneider, H. Britz, **M.I. Titze**, T. Lehr.
A study to assess the accuracy and precision of the digitizing software GetData Graph Digitizer.
Annual meeting of the German Pharmaceutical Society (DPhG), Freiburg, Germany, 2013.

M.I. Titze, M. Ehrhardt, S. Smola, N. Graf, T. Lehr.
A semi-mechanistic model to describe the bidirectional interaction between oncolytic reovirus and in vitro tumor growth of U87-glioblastoma cells.
Annual Meeting of the Population Approach Group in Europe (PAGE), Alicante, Spain, 2014.

M.I. Titze, O. Schaaf, M.H. Hofmann, M.P. Sanderson, S.K. Zahn, J. Quant, T. Lehr.
PK/PD modeling of biomarker modulation and tumor growth inhibition by BI 893923, a novel IGF-1 receptor inhibitor.
Annual Meeting of the Population Approach Group in Europe (PAGE), Hersonissos, Greece, 2015.

M.I. Titze, A. Jonkman, M. Munch, H.M. Lagraauw, P.H. van der Graaf, B. Muller, I. de Greef.
A population disease progression model for Amyotrophic Lateral Sclerosis – Results of the Treeway Summer Challenge 2015.
Annual Meeting of the Population Approach Group in Europe (PAGE), Lisboa, Portugal, 2016.

D. Moj, **M.I. Titze**, T. Lehr.
Pharmacometric Modeling in Clinical Pharmacy – Physiologically-based Pharmacokinetic (PBPK) Modeling.
GradUS Global Meeting, Saarbrücken, Gemany, 2016.

M.I. Titze, D. Moj, T. Lehr.
Pharmacometric Modeling in Clinical Pharmacy – Population Pharmacokinetic Modeling.
GradUS Global Meeting, Saarbrücken, Gemany, 2016.

11.3 Presentations

M.I. Titze.
A semi-mechanistic model to describe the bidirectional interaction between oncolytic reovirus and in vitro tumor growth of U87-glioblastoma cells.
ALDO Summer school 2014, Lyon, France, July 6th-9th, 2014.

M.I. Titze, O. Schaaf.
IGF1R/INSR Inhibitors - Tumor Growth and PK/PD Modeling
IDDS meeting, Vienna, Austria, February 18th, 2014

11.4 Book chapter

D. Moj, **M.I. Titze**, N. Scherer, T. Lehr.
Pharmakogenetik und Therapeutisches Drug Monitoring: Diagnostische Bausteine für die individualisierte Therapie - Kapitel Onkologie
H.-G. Klein, E. Haen, de Gruyter, 2017 (in press).

12 Acknowledgements